Received 30 June 2021; revised 2 August 2021; accepted 3 August 2021. Date of publication 13 August 2021; date of current version 27 August 2021.

*Digital Object Identifier 10.1109/OJCOMS.2021.3103540*

# Defeating Jamming Using Outage Performance Aware Joint Power Allocation and Access Point Placement in Uplink Pairwise NOMA

**VAN-LAN DAO (Graduate Student Member, IEEE), LE-NAM HOANG (Member, IEEE), SVETLANA GIRS (Member, IEEE), AND ELISABETH UHLEMANN (Senior Member, IEEE)**

School of Innovation, Design and Engineering, Malardalen University, 722 20 Västerås, Sweden

CORRESPONDING AUTHOR: V.-L. DAO (e-mail: van.lan.dao@mdh.se)

This work was supported in part by the European Union's Horizon 2020 Research and Innovation Programme through the Marie Skłodowska -Curie, FORA—Fog Computing for Robotics and Industrial Automation under Grant 764785. The work of Le-Nam Hoang and Elisabeth Uhlemann was supported by the Swedish Foundation for Strategic Research through the Serendipity Project.

**ABSTRACT** In this paper, an uplink pairwise Non-Orthogonal Multiple Access (NOMA) scenario using a mobile access point (AP) or an unmanned aerial vehicle in the presence of a jamming attack is considered. To mitigate the influence of the jamming attack, a joint power allocation and AP placement design is proposed. Accordingly, closed-form expressions of the overall outage probability (OOP) and the individual outage probability (IOP) considering imperfect channel state information for each of the source nodes the AP serves, are derived over Nakagami-*m* fading channels using dynamic decoding order and fixed pairwise power allocation. We conduct an investigation of the effect of different parameters such as power allocation, source node placements, AP placement, target rates, and jammer location on the OOP and the IOP performance. By adapting the power allocation and the AP placement to the jamming attack, the communication reliability can be increased significantly compared to neglecting the presence of the jammer or treating the jammer as noise. Since the malicious jammer and the AP have conflicting interests in terms of communication reliability, we formulate a non-cooperative game for the two players considering their positions and the power allocation of the NOMA nodes as their strategies and the OOP as utility function. We propose using hybrid simulated annealing - greedy algorithms to address the joint power allocation and AP placement problem for the cases of both a fixed and a mobile jammer. Finally, the Nash equilibrium points are obtained and then the UAV goes directly to this position and keeps staying there to save power consumption.

**INDEX TERMS** Dynamic decoding order, imperfect CSI, outage performance, UAV placement, pairwise NOMA, game theory, metaheuristic optimization.

## I. INTRODUCTION

RECENTLY, mobile access points (APs), i.e., APs mounted on a mobile device, have been adopted in many applications such as communication among mobile robots, vehicles or unmanned aerial vehicle (UAV) aided networks [1], [2]. Placing an AP on, e.g., a UAV brings several benefits in terms of mobility and adaptive altitude, flexibility, adjustable usage and effortless deployment. UAV based networks have been considered as a promising solution for a wide range of applications including both civil and military uses [2], [3], e.g., healthcare [4], disaster communication [5], smart factories [6] and precision agriculture [7]. However, this new broader set of applications increases the requirements on ultra-high reliability, low latency, and high connectivity [8], [9]. Delays caused by waiting for channel access, or reliability problems due to collisions when several nodes are attempting to access the channel at the same time, severely affect the performance. In order to address these issues, Non-Orthogonal Multiple Access (NOMA) is a potential solution for industrial applications as well as for 6G and beyond [10]–[12]. As it is shown in [13], NOMA can

help improving both latency and throughput compared to Orthogonal Multiple Access (OMA). Pairwise NOMA can also be used in combination with an existing multiple access technology like Time Division Multiple Access (TDMA) to increase the number of nodes that can get access to the channel at each time instance. Moreover, in industrial automation, the NOMA-based systems in [14] are shown to be more predictable and provide higher reliability for the critical-service users than TDMA, even though the performance of the best-effort user has to be sacrificed a little. However, due to the complex nature of the successive interference cancellation (SIC) operation and the imperfect SIC experienced in practice, the number of nodes that are served simultaneously should not be too large [15], which makes pairwise NOMA a more practical option considering also hardware implementation [15], [16]. Therefore, using a mobile AP or a UAV in pairwise NOMA is a potential solution in many emerging scenarios of practical importance.

Although wireless networks offer a huge number of advantages such as mobility, flexibility, scalability, lower cost and less delay for installation and updating, wireless transmissions are more vulnerable to jamming attacks due to the inherent open nature of wireless communication [17]–[19]. In fact, jamming and also co-operative attacks can severely interrupt legitimate ongoing transmissions. As an example, National Institute of Standards and Technology (NIST) reported a detected vulnerability towards jamming attacks according to *"An issue was discovered on ABUS Secvest FUAA50000 3.01.01 devices. Due to an insufficient implementation of jamming detection, an attacker is able to suppress correctly received RF messages sent between wireless peripheral components, e.g., wireless detectors or remote controls, and the ABUS Secvest alarm central. An attacker is able to perform a "reactive jamming" attack."* [20]. Therefore, cyber-security in terms of defeating jamming attacks has become urgent given the strict application requirements [21]–[25]. Moreover, the significant increase in the number of connected devices leads to a situation where spectrum reuse and dense deployment are unavoidable [26]. This in turn leads to different wireless networks interfering with others. Therefore, interference management must be considered [27]–[29] and, more importantly, the system models must take jamming attacks in terms of any type of interference or malicious jamming into account.

In the literature, anti jamming attacks have attracted a lot of attention from researchers in both civil and military applications, e.g., [18]. However, there are rather few previous studies on anti jamming attacks and how they affect the outage performance, especially in networks relying on power allocation and channel estimation like NOMA. In [19], [30], a cooperative attack between a malicious jammer and an eavesdropper is introduced in the context that the locations of all nodes are fixed. However, these works do not show how to choose the power allocation while dealing with the jamming attack to maximize the communication reliability. To alleviate a harmful jamming attack, the authors in [31] introduce a novel anti jamming precoding design with the constraint of minimizing the total transmit power, in which all nodes have fixed locations as well. In real scenarios, jammers are also smart and can change their positions to effectively defeat the legal communication system, but the aforementioned publications only considered fixed jammers' placement [32]–[36]. It should also be noted that these fixed positions are not optimal for the jammers. Moreover, the UAV can also adapt to change its placement to mitigate jamming [37], [38]. However, no previous work has considered the UAV placement as a part of the strategy to defeat a jamming attack in pairwise NOMA. Note that for downlink scenarios, when the UAV acts as transmitter, the UAV placement can be derived quite trivially even in a jamming scenario since the goal is to maximize the reliability for the source node most affected by the jammer. However, in the uplink, when the UAV acts as receiver, the power allocation and the UAV placement are non-trivial and both very important to mitigate a jamming attack. Hence, this paper focuses on uplink pairwise NOMA.

In this paper we target industrial wireless networks, where reliability and latency requirements have higher priority than others, e.g., throughput and power consumption [39]. If the transmitted packets do not reach the destinations before the deadline with a given reliability level, problems with safety and functional requirements occur. At the system level, deadline misses can cause the applications to fail, leading to economic loss or serious safety problems. Therefore, in this paper, the outage probabilities consisting of both individual outage probability (IOP) and overall outage probability (OOP) are used to evaluate the communication reliability of the legitimate wireless UAV communication system in the presence of a jamming attack in uplink pairwise NOMA. Further, since both source nodes are served simultaneously in uplink pairwise NOMA, user fairness is also an important performance measure. While the OOP can be used to evaluate the performance of larger wireless networks supporting short-term user fairness, the IOP is best suited for evaluating the communication reliability of individual nodes. In [16], the OOP is derived with perfect channel state information (CSI) and without a jamming attack, and it is noted that if there exists any type of interferer which can be considered as noise, the OOP can be obtained directly from the OOP in [16]. However, in the presence of a jamming attack, the OOP cannot be derived directly from the obtained OOP in [16] because there exists multipath fading between the UAV and the jammer. Moreover, the estimated CSIs at the UAV are imperfect in this situation. Thus, new closed-form expressions are needed specifically for the case of a jamming attack.

The aforementioned problems motivate us to look at a joint power allocation and UAV location design taking all node placements, the jammer location, the power allocation strategy and imperfect CSI into account, while using a dynamic decoding order and a fixed pairwise power allocation scheme to maximize the communication reliability of

the legal wireless communication system. Moreover, the conflicting interests between the malicious jammer and the UAV based on their purposes can be formulated as a competition game to provide more insightful discussions on how to meet the strict reliability requirements for specific applications as well as making suitable pairs of source nodes. Consequently, the main contributions of this work can be summarized as follows:

- Taking the jamming attack and imperfect CSI into account, the exact closed-form expressions of both OOP and IOP for each source node are derived.
- Using these closed-form expressions, an investigation of the effect of some parameters on the OOP and IOP such as power allocation, source node placements, UAV placement, target rates, and jammer location is conducted. Moreover, we show that by tuning the power allocation and the UAV placement in accordance to the jamming attack, the communication reliability is improved significantly compared to neglecting the presence of the jammer or treating the jammer as noise.
- By formulating a competition game between the UAV and the jammer considering their positions and power allocation to the NOMA nodes as their strategies and the OOP as a utility function, we show that eventually a Nash equilibrium will be reached in both the fixed and the mobile jammer scenarios.
- To attain the equilibrium points as well as optimal power allocation and UAV placement under the strict timing constraint, we propose a set of hybrid Simulated Annealing (SA)-Greedy algorithms.

The rest of this paper is organized as follows: The system model is described in Section II. Then, Section III presents the calculation of the OOP and IOP for each source node in uplink pairwise NOMA. Thereafter, a joint power allocation and UAV placement design for both fixed and mobile jammer scenarios is provided in Section IV, in which non-cooperative games are formulated for both scenarios of using a fixed and a mobile jammer. Next, numerical results and discussions are presented in Section V. Finally, Section VI concludes the paper.

## II. SYSTEM MODEL

In industrial applications, wireless networks and other infrastructure are designed, positioned, and controlled by the organizations owning them. In other words, jamming attacks appearing inside the legitimate area are less likely and are handled by other types of physical protection like fences or walls. Hence, jammers are typically restricted to staying at any place outside of the border to attack the legal communication system. Still, the situation when both source nodes and a smart jammer are staying close to the border, may dramatically degrade the communication reliability.

Dealing with a jamming attack in uplink NOMA is different compared to downlink. Consider the example of a jamming attack including a mobile AP, two source nodes with fixed positions, and a mobile jammer, in which the

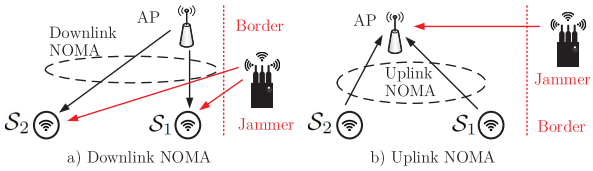


**FIGURE 1.** A scenario of jamming attack in both uplink and downlink NOMA.

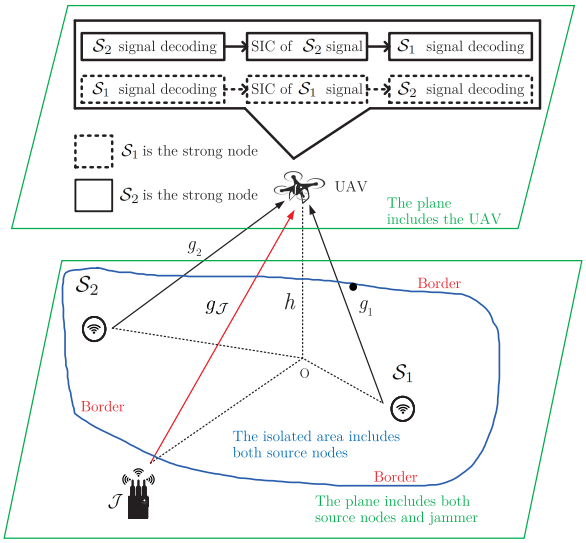


**FIGURE 2.** System model.

legitimate area is protected inside of the border as shown in Fig. 1. Note that $\mathcal{S}_1$ is located close to the border, while the another source node stays far away from the border. In downlink NOMA, the AP should stay close to $\mathcal{S}_1$ to make the channel between the AP and $\mathcal{S}_1$ better, e.g., the UAV should stay on top of $\mathcal{S}_1$ [40]. In contrast, in uplink NOMA, the AP is the receiver and if it should stay close to $\mathcal{S}_1$ in this case, it would be bad as this is the position most affected by the jammer. Whereas the UAV placement can be derived quite trivially for jamming in the downlink, the power allocation and the AP placement are both very important to mitigate a jamming attack in uplink NOMA.

We therefore consider a system consisting of two source nodes $\mathcal{S}_i$, $i \in \{1, 2\}$ communicating with a mobile AP, or a UAV, in uplink pairwise NOMA, Fig. 2. There also exists a malicious jammer $\mathcal{J}$ generating jamming signal over all channels to attack the UAV. Note that an interferer located nearby the system can also be modeled as a jammer, but operating with very low transmit power, e.g., 1mW. Here, $h$ is the distance between the UAV and the plane consisting of both source nodes and the jammer. To have a generic model for the channels between the AP and other nodes, we use a channel model considering both fading and path-loss [41]–[43]. Accordingly, channels between the UAV and $\mathcal{S}_i$ and between $\mathcal{J}$ and the UAV are $\widetilde{g}_i = \frac{g_i}{\sqrt{1+d_i^{\zeta_i}}}$ and $\widetilde{g}_{\mathcal{J}} = \frac{g_{\mathcal{J}}}{\sqrt{1+d_{\mathcal{J}}^{\zeta_{\mathcal{J}}}}}$ [42], respectively. Here, the channel coefficients $g_i$ and $g_{\mathcal{J}}$ are

assumed to be Nakagami-$m$ fading, modeling a large number of wireless channels by adjusting its parameters, e.g., Rayleigh fading with $m = 1$, Rician fading with parameter $K$ when $m = \frac{(K+1)^2}{2K+1}$ [44]. $d_i$ and $d_{\mathcal{J}}$ are the distances between the UAV and $\mathcal{S}_i$ and between $\mathcal{J}$ and the UAV, respectively; $\zeta_i$ and $\zeta_{\mathcal{J}}$ are the path-loss exponents of the channel between $\mathcal{S}_i$ and the UAV and between the UAV and $\mathcal{J}$, respectively. We consider that all users operate in half-duplex mode with a single antenna. Moreover, the UAV, $\mathcal{S}_i$, and $\mathcal{J}$ are located at $(x_u, y_u, h)$, $(x_i, y_i, 0)$, and $(x_{\mathcal{J}}, y_{\mathcal{J}}, 0)$, respectively. We also assume that both users are located in the isolated area, while the jammer is only allowed to appear outside of the border, Fig. 2. Accordingly, the distance between the UAV and $\mathcal{S}_i$ and the UAV and $\mathcal{J}$ can be expressed as follows:

$$d_i = \sqrt{h^2 + (x_i - x_u)^2 + (y_i - y_u)^2}, \tag{1}$$

$$d_{\mathcal{J}} = \sqrt{h^2 + \left(x_{\mathcal{J}} - x_u\right)^2 + \left(y_{\mathcal{J}} - y_u\right)^2}. \tag{2}$$

In this work we take imperfect CSI into account. The channel coefficients between the UAV and $\mathcal{S}_i$ using linear minimum mean square error are represented as $g_i = \widehat{g}_i + e_i$. Therefore, the channels between the UAV and $\mathcal{S}_i$ can be given as

$$\widetilde{g}_i = \frac{\widehat{g}_i + e_i}{\sqrt{1 + d_i^{\zeta_i}}}, \tag{3}$$

where $\widehat{g}_i$ and $e_i \sim CN(0, \sigma_i^2)$ are the estimated channel coefficient and channel estimation error, respectively. It is noticed that $\widehat{g}_i$ and $e_i$ are uncorrelated. This is because of the orthogonality principle of linear minimum mean square error algorithm. Furthermore, the channels between the UAV and $\mathcal{S}_i$ and the UAV and $\mathcal{J}$ follow Nakagami-$m$ fading, therefore channel gains $|\widehat{g}_i|^2$ and $|g_{\mathcal{J}}|^2$ can also be characterized by a Gamma distribution with unit mean and shape $m_i$ and $m_{\mathcal{J}}$, respectively. Here, we only consider that the channel estimation errors are fixed and independent compared to the average signal-to-noise ratio (SNR).

Following the channel estimation error mode in [45], the received signal at the UAV can be represented as follows:

$$y = \sum_{i=1}^{2} \frac{\widehat{g}_i + e_i}{\sqrt{1 + d_i^{\zeta_i}}} \sqrt{P_i} z_i + \frac{g_{\mathcal{J}}}{\sqrt{1 + d_{\mathcal{J}}^{\zeta_{\mathcal{J}}}}} \sqrt{P_{\mathcal{J}}} z_{\mathcal{J}} + n, \tag{4}$$

where $P$, $P_{\mathcal{J}}$, $P_i$, $z_i$, $z_{\mathcal{J}}$, and $n$ are the total transmit power of both source nodes, transmit power of the jammer, power allocation level for each source node $\mathcal{S}_i$, uplink signal of $\mathcal{S}_i$, noise signal of the jamming attack, and additive white Gaussian noise at the UAV modeled as $n \sim CN(0, \sigma_0^2)$, respectively. Note that $P_1 + P_2 = P$. Moreover, the UAV adopts the estimated channel coefficients between the UAV and $\mathcal{S}_i$ to decide on decoding order.

In both uplink and downlink NOMA, the authors in [46] show that power allocation plays an important role and affects the system performance significantly. They also clarify that the power allocation significantly influences the decoding order in downlink NOMA, while the decoding order in uplink NOMA is decided based on both the power allocation and the channel gains. Moreover, a dynamic decoding order offers higher reliability compared to a fixed decoding order [16], [47], [48]. Therefore, we use the dynamic decoding order and fixed pairwise power allocation scheme proposed in [16] in this work, to reduce the complexity of the communication protocol without degrading the OOP. Define $h_i = \rho_i |\widehat{g}_i|^2$, $\rho_i = \frac{P}{W\sigma_0^2(1+d_i^{\zeta_i})}$, $h_{\mathcal{J}} = \rho_{\mathcal{J}} |g_{\mathcal{J}}|^2$, $\rho_{\mathcal{J}} = \frac{P_{\mathcal{J}}}{W\sigma_0^2(1+d_{\mathcal{J}}^{\zeta_{\mathcal{J}}})}$, where $W$ is the system bandwidth. With $h_1 \geq h_2$, $\mathcal{S}_1$'s signal is decoded directly by considering both $\mathcal{S}_2$'s signal and $\mathcal{J}$'s signal as interference and then subtracted by SIC from the received signal $y$ before decoding $\mathcal{S}_2$'s signal treating $\mathcal{J}$'s signal as interference. Accordingly, the received signal-to-interference-plus-noise ratios (SINRs) at the UAV to decode $z_1$ and $z_2$ can be represented as follows:

$$\gamma_1 = \frac{\mu_1 h_1}{\mu_2 h_2 + h_{\mathcal{J}} + \mu_1 \sigma_1^2 \rho_1 + \mu_2 \sigma_2^2 \rho_2 + 1}, \tag{5}$$

$$\gamma_2 = \frac{\mu_2 h_2}{h_{\mathcal{J}} + \mu_1 \sigma_1^2 \rho_1 + \mu_2 \sigma_2^2 \rho_2 + 1}, \tag{6}$$

where $0 < \mu_i < 1$ is the power allocation factor for $\mathcal{S}_i$, $\mu_1 + \mu_2 = 1$. In contrast, with $h_1 < h_2$, $\mathcal{S}_2$'s signal is decoded first before decoding $\mathcal{S}_1$'s signal, thus the received SINRs at the UAV to decode $z_2$ and $z_1$ can be formulated as

$$\gamma_2^{'} = \frac{\mu_2^{'} h_2}{\mu_1^{'} h_1 + h_{\mathcal{J}} + \mu_1^{'} \sigma_1^2 \rho_1 + \mu_2^{'} \sigma_2^2 \rho_2 + 1}, \tag{7}$$

$$\gamma_1^{'} = \frac{\mu_1^{'} h_1}{h_{\mathcal{J}} + \mu_1^{'} \sigma_1^2 \rho_1 + \mu_2^{'} \sigma_2^2 \rho_2 + 1}, \tag{8}$$

where $0 < \mu_i^{'} < 1$ is the power level for $\mathcal{S}_i$, $\mu_1^{'} + \mu_2^{'} = 1$. It is noticed that $(\mu_1^{'}, \mu_2^{'})$ is able to be different from $(\mu_1, \mu_2)$. To inform the two sources about which fixed power allocation to use, the UAV can, e.g., employ individual control channels [49]. This process is much less complex compared to sending the power allocation factors as payload data.

## III. OUTAGE PERFORMANCE ANALYSIS

In this section, we analyze situations when an event of outage occurs and consequently derive the exact closed-form expressions of both OOP and IOP for each source node. The detailed calculation refers to the theorem given in the Appendix.

### A. OVERALL OUTAGE PROBABILITY

The system is in outage when at least one signal of the two source nodes is not decoded correctly at the UAV. Accordingly, the OOP can be determined as follows:

$$p = 1 - I_1 - I_2, \tag{9}$$

in which $I_1$ is the joint probability of successful decoding $\mathcal{S}_1$'s signal treating other signals including $\mathcal{S}_2$'s signal and $\mathcal{J}$'s signal as interference and then removing $\mathcal{S}_1$'s signal from the received signal $y$ before decoding correctly the

$\mathcal{S}_2$'s signal with interference of $\mathcal{J}$ at the UAV in the case of $h_1 \geq h_2$. In contrast, $I_2$ is the joint probability of correct decoding $\mathcal{S}_2$'s signal considering $\mathcal{S}_1$'s signal and $\mathcal{J}$'s signal as interference and then subtracting $\mathcal{S}_2$'s signal from the received signal $y$ before decoding exactly the $\mathcal{S}_1$'s signal treating $\mathcal{J}$'s signal as interference at the UAV when $h_1 < h_2$. Consequently, $I_1$ and $I_2$ are defined as follows:

$$\begin{aligned} I_1 &= \Pr\{(\gamma_1 \geq A_1) \cap (\gamma_2 \geq A_2) \cap (h_1 \geq h_2)\} \\ &= \Pr\left\{\left(\frac{\mu_1 h_1}{\mu_2 h_2 + h_{\mathcal{J}} + a_0} \geq A_1\right) \cap (h_1 \geq h_2) \right. \\ &\qquad \left. \cap\left(\frac{\mu_2 h_2}{h_{\mathcal{J}} + a_0} \geq A_2\right)\right\}, \end{aligned} \tag{10}$$

$$\begin{aligned} I_2 &= \Pr\left\{\left(\gamma_1^{'} \geq A_1\right) \cap \left(\gamma_2^{'} \geq A_2\right) \cap (h_1 < h_2)\right\} \\ &= \Pr\left\{\left(\frac{\mu_1^{'} h_1}{h_{\mathcal{J}} + b_0} \geq A_1\right) \cap (h_1 < h_2) \right. \\ &\qquad \left. \cap\left(\frac{\mu_2^{'} h_2}{\mu_1^{'} h_1 + h_{\mathcal{J}} + b_0} \geq A_2\right)\right\}, \end{aligned} \tag{11}$$

where $a_0 = \mu_1\sigma_1^2\rho_1 + \mu_2\sigma_2^2\rho_2 + 1$ and $b_0 = \mu_1'\sigma_1^2\rho_1 + \mu_2'\sigma_2^2\rho_2 + 1$, $A_1 = 2^{\frac{R_{1th}}{W}} - 1$, $A_2 = 2^{\frac{R_{2th}}{W}} - 1$, in which $R_{1th}$ and $R_{2th}$ are the target rates of $\mathcal{S}_1$ and $\mathcal{S}_2$, respectively. Taking all possible cases into account, we can re-write the probabilities $I_1$ and $I_2$ as follows:

$$I_1 = \begin{cases} I_{10} & \mu_2 A_1 \geq \mu_1 \\ I_{11} + I_{12} & \text{otherwise}, \end{cases} \tag{12}$$

$$I_2 = \begin{cases} I_{20} & \mu_1' A_2 \geq \mu_2' \\ I_{21} + I_{22} & \text{otherwise}, \end{cases} \tag{13}$$

in which $I_{10}$, $I_{11}$, $I_{12}$, $I_{20}$, $I_{21}$, and $I_{22}$ are given as

$$I_{10} = \Pr\left\{\begin{matrix}(h_1 \geq a_1 h_2 + a_2 h_{\mathcal{J}} + a_3) \\ \cap(h_2 \geq a_4 h_{\mathcal{J}} + a_5)\end{matrix}\right\}, \tag{14}$$

$$I_{11} = \Pr\left\{\begin{matrix}(h_2 \leq a_6 h_{\mathcal{J}} + a_7) \\ \cap(h_2 \geq a_4 h_{\mathcal{J}} + a_5) \\ \cap(h_1 \geq a_1 h_2 + a_2 h_{\mathcal{J}} + a_3)\end{matrix}\right\}, \tag{15}$$

$$I_{12} = \Pr\left\{\begin{matrix}(h_1 \geq h_2) \cap (h_2 \geq a_4 h_{\mathcal{J}} + a_5) \\ \cap(h_2 > a_6 h_{\mathcal{J}} + a_7)\end{matrix}\right\}, \tag{16}$$

$$I_{20} = \Pr\left\{\begin{matrix}(h_2 \geq b_1 h_1 + b_2 h_{\mathcal{J}} + b_3) \\ \cap(h_1 \geq b_4 h_{\mathcal{J}} + b_5)\end{matrix}\right\}, \tag{17}$$

$$I_{21} = \Pr\left\{\begin{matrix}(h_2 \geq b_1 h_1 + b_2 h_{\mathcal{J}} + b_3) \\ \cap(h_1 \geq b_4 h_{\mathcal{J}} + b_5) \\ \cap(h_1 \leq b_6 h_{\mathcal{J}} + b_7)\end{matrix}\right\}, \tag{18}$$

$$I_{22} = \Pr\left\{\begin{matrix}(h_2 > h_1) \cap (h_1 \geq b_4 h_{\mathcal{J}} + b_5) \\ \cap(h_1 > b_6 h_{\mathcal{J}} + b_7)\end{matrix}\right\}, \tag{19}$$

where $a_1 = \frac{\mu_2 A_1}{\mu_1}$, $a_2 = \frac{A_1}{\mu_1}$, $a_3 = \frac{A_1 a_0}{\mu_1}$, $a_4 = \frac{A_2}{\mu_2}$, $a_5 = \frac{a_0 A_2}{\mu_2}$, $a_6 = \frac{A_1}{\mu_1 - \mu_2 A_1}$, $a_7 = \frac{A_1 a_0}{\mu_1 - \mu_2 A_1}$, $b_1 = \frac{A_2 \mu_1'}{\mu_2'}$, $b_2 = \frac{A_2}{\mu_2'}$, $b_3 = \frac{b_0 A_2}{\mu_2'}$, $b_4 = \frac{A_1}{\mu_1'}$, $b_5 = \frac{b_0 A_1}{\mu_1'}$, $b_6 = \frac{A_2}{\mu_2' - A_2\mu_1'}$, $b_7 = \frac{b_0 A_2}{\mu_2' - A_2\mu_1'}$. In fact, the closed-form expressions of $I_{11}$, $I_{12}$, $I_{21}$, and $I_{22}$ cannot be derived by directly applying Theorem 2. Therefore, we use Venn diagrams to separate them into some sub-cases. Then $I_{10}, I_{11}, I_{12}, I_{20}, I_{21}$, and $I_{22}$ are derived in the following lemma.

*Lemma 1:* Given that $h_i \sim G(m_i, \frac{\rho_i}{m_i})$ and $h_{\mathcal{J}} \sim G(m_{\mathcal{J}}, \frac{\rho_{\mathcal{J}}}{m_{\mathcal{J}}})$, the closed-form expressions of $I_{10}$, $I_{11}$, $I_{12}$, $I_{20}$, $I_{21}$, and $I_{22}$ can be obtained as follows:

$$\begin{aligned} I_{10} = &\frac{\left(m_2\rho_2^{-1}\right)^{m_2}\left(m_{\mathcal{J}}\rho_{\mathcal{J}}^{-1}\right)^{m_{\mathcal{J}}} e^{-m_1\rho_1^{-1}a_3 - B_1 a_5}}{\Gamma(m_{\mathcal{J}})\Gamma(m_2)} \\ &\times \sum_{i=0}^{m_1-1} \frac{\left(m_1\rho_1^{-1}\right)^i}{i!} \sum_{j=0}^{i} \binom{i}{j} \frac{a_1^j \Gamma(m_2 + j)}{B_1^{m_2+j}} \sum_{k=0}^{i-j} a_3^{i-j-k} a_2^k \\ &\times \binom{i-j}{k} \sum_{l=0}^{m_2+j-1} \frac{B_1^l}{l!} \sum_{q=0}^{l} \binom{l}{q} a_5^{l-q} a_4^q \frac{\Gamma(m_{\mathcal{J}} + k + q)}{B_2^{m_{\mathcal{J}}+k+q}}, \end{aligned} \tag{20}$$

$$I_{11} = \begin{cases} I_{11a} & a_5 < a_7, x_1 \leq 0 \\ I_{11b} & a_5 \geq a_7, x_1 > 0 \\ 0 & a_5 \geq a_7, x_1 \leq 0 \\ I_{11a} - I_{11b} & a_5 < a_7, x_1 > 0, \end{cases} \tag{21}$$

in which $I_{11a}$, and $I_{11b}$ are given as

$$\begin{aligned} I_{11a} = I_{10} - &\frac{\left(m_2\rho_2^{-1}\right)^{m_2}\left(m_{\mathcal{J}}\rho_{\mathcal{J}}^{-1}\right)^{m_{\mathcal{J}}} e^{-m_1\rho_1^{-1}a_3 - B_1 a_7}}{\Gamma(m_{\mathcal{J}})\Gamma(m_2)} \\ &\times \sum_{i=0}^{m_1-1} \frac{\left(m_1\rho_1^{-1}\right)^i}{i!} \sum_{j=0}^{i} \binom{i}{j} \frac{a_1^j \Gamma(m_2 + j)}{B_1^{m_2+j}} \sum_{k=0}^{i-j} a_3^{i-j-k} a_2^k \\ &\times \binom{i-j}{k} \sum_{l=0}^{m_2+j-1} \frac{B_1^l}{l!} \sum_{q=0}^{l} \binom{l}{q} a_7^{l-q} a_6^q \\ &\times \frac{\Gamma(m_{\mathcal{J}} + k + q)}{B_3^{m_{\mathcal{J}}+k+q}}, \end{aligned} \tag{22}$$

$$\begin{aligned} I_{11b} = &\frac{\left(m_2\rho_2^{-1}\right)^{m_2}\left(m_{\mathcal{J}}\rho_{\mathcal{J}}^{-1}\right)^{m_{\mathcal{J}}} e^{-m_1\rho_1^{-1}a_3 - B_1 a_5}}{\Gamma(m_{\mathcal{J}})\Gamma(m_2)} \\ &\times \sum_{i=0}^{m_1-1} \frac{\left(m_1\rho_1^{-1}\right)^i}{i!} \sum_{j=0}^{i} \binom{i}{j} \frac{a_1^j \Gamma(m_2 + j)}{B_1^{m_2+j}} \sum_{k=0}^{i-j} a_3^{i-j-k} a_2^k \\ &\times \binom{i-j}{k} \sum_{l=0}^{m_2+j-1} \frac{B_1^l}{l!} \sum_{q=0}^{l} \binom{l}{q} a_5^{l-q} a_4^q \\ &\times \frac{\Gamma(m_{\mathcal{J}} + k + q, B_2 x_1)}{B_2^{m_{\mathcal{J}}+k+q}} \\ &- \frac{\left(m_2\rho_2^{-1}\right)^{m_2}\left(m_{\mathcal{J}}\rho_{\mathcal{J}}^{-1}\right)^{m_{\mathcal{J}}} e^{-m_1\rho_1^{-1}a_3 - B_1 a_7}}{\Gamma(m_{\mathcal{J}})\Gamma(m_2)} \\ &\times \sum_{i=0}^{m_1-1} \frac{\left(m_1\rho_1^{-1}\right)^i}{i!} \sum_{j=0}^{i} \binom{i}{j} \frac{a_1^j \Gamma(m_2 + j)}{B_1^{m_2+j}} \sum_{k=0}^{i-j} a_3^{i-j-k} a_2^k \end{aligned} \tag{23}$$

$$\times \binom{i-j}{k} \sum_{l=0}^{m_2+j-1} \frac{B_1^l}{l!} \sum_{q=0}^{l} \binom{l}{q} a_7^{l-q} a_6^q \times \frac{\Gamma\left(m_{\mathcal{J}}+k+q, B_3 x_1\right)}{B_3^{m_{\mathcal{J}}+k+q}},$$

$$I_{12} = \begin{cases} I_{12a} & a_5 \geq a_7, x_1 \leq 0 \\ I_{12b} & a_5 < a_7, x_1 \leq 0 \\ I_{12a} - Q_1 & a_5 \geq a_7, x_1 > 0 \\ I_{12b} + Q_1 & a_5 < a_7, x_1 > 0, \end{cases} \tag{24}$$

in which $I_{12a}$, $I_{12b}$ and $Q_1$ are given as

$$I_{12a} = \frac{\left(m_2\rho_2^{-1}\right)^{m_2}\left(m_{\mathcal{J}}\rho_{\mathcal{J}}^{-1}\right)^{m_{\mathcal{J}}} e^{-B_4 a_5}}{\Gamma\left(m_{\mathcal{J}}\right)\Gamma(m_2)} \times \sum_{j=0}^{m_1-1} \frac{\left(m_1\rho_1^{-1}\right)^j \Gamma(m_2+j)}{j! B_4^{m_2+j}} \sum_{l=0}^{m_2+j-1} \frac{B_4^l}{l!} \times \sum_{q=0}^{l} \binom{l}{q} a_4^q a_5^{l-q} \frac{\Gamma\left(m_{\mathcal{J}}+q\right)}{B_5^{m_{\mathcal{J}}+q}}, \tag{25}$$

$$I_{12b} = \frac{\left(m_2\rho_2^{-1}\right)^{m_2}\left(m_{\mathcal{J}}\rho_{\mathcal{J}}^{-1}\right)^{m_{\mathcal{J}}} e^{-B_4 a_7}}{\Gamma\left(m_{\mathcal{J}}\right)\Gamma(m_2)} \times \sum_{j=0}^{m_1-1} \frac{\left(m_1\rho_1^{-1}\right)^j \Gamma(m_2+j)}{j! B_4^{m_2+j}} \sum_{l=0}^{m_2+j-1} \frac{B_4^l}{l!} \times \sum_{q=0}^{l} \binom{l}{q} a_6^q a_7^{l-q} \frac{\Gamma\left(m_{\mathcal{J}}+q\right)}{B_6^{m_{\mathcal{J}}+q}}, \tag{26}$$

$$Q_1 = \frac{\left(m_2\rho_2^{-1}\right)^{m_2}\left(m_{\mathcal{J}}\rho_{\mathcal{J}}^{-1}\right)^{m_{\mathcal{J}}} e^{-B_4 a_5}}{\Gamma\left(m_{\mathcal{J}}\right)\Gamma(m_2)} \times \sum_{j=0}^{m_1-1} \frac{\left(m_1\rho_1^{-1}\right)^j \Gamma(m_2+j)}{j! B_4^{m_2+j}} \sum_{l=0}^{m_2+j-1} \frac{B_4^l}{l!} \times \sum_{q=0}^{l} \binom{l}{q} a_4^q a_5^{l-q} \frac{\Gamma\left(m_{\mathcal{J}}+q, B_5 x_1\right)}{B_5^{m_{\mathcal{J}}+q}} - \frac{\left(m_2\rho_2^{-1}\right)^{m_2}\left(m_{\mathcal{J}}\rho_{\mathcal{J}}^{-1}\right)^{m_{\mathcal{J}}} e^{-B_4 a_7}}{\Gamma\left(m_{\mathcal{J}}\right)\Gamma(m_2)} \times \sum_{j=0}^{m_1-1} \frac{\left(m_1\rho_1^{-1}\right)^j \Gamma(m_2+j)}{j! B_4^{m_2+j}} \sum_{l=0}^{m_2+j-1} \frac{B_4^l}{l!} \times \sum_{q=0}^{l} \binom{l}{q} a_6^q a_7^{l-q} \frac{\Gamma\left(m_{\mathcal{J}}+q, B_6 x_1\right)}{B_6^{m_{\mathcal{J}}+q}}, \tag{27}$$

$$I_{20} = \frac{\left(m_1\rho_1^{-1}\right)^{m_1}\left(m_{\mathcal{J}}\rho_{\mathcal{J}}^{-1}\right)^{m_{\mathcal{J}}} e^{-m_2\rho_2^{-1}b_3 - B_7 b_5}}{\Gamma\left(m_{\mathcal{J}}\right)\Gamma(m_1)} \times \sum_{i=0}^{m_2-1} \frac{\left(m_2\rho_2^{-1}\right)^i}{i!} \sum_{j=0}^{i} \binom{i}{j} \frac{b_1^j \Gamma(m_1+j)}{B_7^{m_1+j}} \sum_{k=0}^{i-j} b_3^{i-j-k} b_2^k$$

$$\times \binom{i-j}{k} \sum_{l=0}^{m_1+j-1} \frac{B_7^l}{l!} \sum_{q=0}^{l} \binom{l}{q} b_5^{l-q} b_4^q \times \frac{\Gamma\left(m_{\mathcal{J}}+k+q\right)}{B_8^{m_{\mathcal{J}}+k+q}}, \tag{28}$$

$$I_{21} = \begin{cases} I_{21a} & b_5 < b_7, x_2 \leq 0 \\ I_{21b} & b_5 \geq b_7, x_2 > 0 \\ 0 & b_5 \geq b_7, x_2 \leq 0 \\ I_{21a} - I_{21b} & b_5 < b_7, x_2 > 0, \end{cases} \tag{29}$$

in which $I_{21a}$ and $I_{21b}$ are given as

$$I_{21a} = I_{20} - \frac{\left(m_1\rho_1^{-1}\right)^{m_1}\left(m_{\mathcal{J}}\rho_{\mathcal{J}}^{-1}\right)^{m_{\mathcal{J}}} e^{-m_2\rho_2^{-1}b_3 - B_7 b_7}}{\Gamma\left(m_{\mathcal{J}}\right)\Gamma(m_1)} \times \sum_{i=0}^{m_2-1} \frac{\left(m_2\rho_2^{-1}\right)^i}{i!} \sum_{j=0}^{i} \binom{i}{j} \frac{b_1^j \Gamma(m_1+j)}{B_7^{m_1+j}} \sum_{k=0}^{i-j} b_3^{i-j-k} b_2^k \times \binom{i-j}{k} \sum_{l=0}^{m_1+j-1} \frac{B_7^l}{l!} \sum_{q=0}^{l} \binom{l}{q} b_7^{l-q} b_6^q \times \frac{\Gamma\left(m_{\mathcal{J}}+k+q\right)}{B_9^{m_{\mathcal{J}}+k+q}}, \tag{30}$$

$$I_{21b} = \frac{\left(m_1\rho_1^{-1}\right)^{m_1}\left(m_{\mathcal{J}}\rho_{\mathcal{J}}^{-1}\right)^{m_{\mathcal{J}}} e^{-m_2\rho_2^{-1}b_3 - B_7 b_5}}{\Gamma\left(m_{\mathcal{J}}\right)\Gamma(m_1)} \times \sum_{i=0}^{m_2-1} \frac{\left(m_2\rho_2^{-1}\right)^i}{i!} \sum_{j=0}^{i} \binom{i}{j} \frac{b_1^j \Gamma(m_1+j)}{B_7^{m_1+j}} \sum_{k=0}^{i-j} b_3^{i-j-k} b_2^k \times \binom{i-j}{k} \sum_{l=0}^{m_1+j-1} \frac{B_7^l}{l!} \sum_{q=0}^{l} \binom{l}{q} b_5^{l-q} b_4^q \times \frac{\Gamma\left(m_{\mathcal{J}}+k+q, B_8 x_2\right)}{B_8^{m_{\mathcal{J}}+k+q}} - \frac{\left(m_1\rho_1^{-1}\right)^{m_1}\left(m_{\mathcal{J}}\rho_{\mathcal{J}}^{-1}\right)^{m_{\mathcal{J}}} e^{-m_2\rho_2^{-1}b_3 - B_7 b_7}}{\Gamma\left(m_{\mathcal{J}}\right)\Gamma(m_1)} \times \sum_{i=0}^{m_2-1} \frac{\left(m_2\rho_2^{-1}\right)^i}{i!} \sum_{j=0}^{i} \binom{i}{j} \frac{b_1^j \Gamma(m_1+j)}{B_7^{m_1+j}} \sum_{k=0}^{i-j} b_3^{i-j-k} b_2^k \times \binom{i-j}{k} \sum_{l=0}^{m_1+j-1} \frac{B_7^l}{l!} \sum_{q=0}^{l} \binom{l}{q} b_7^{l-q} b_6^q \times \frac{\Gamma\left(m_{\mathcal{J}}+k+q, B_9 x_2\right)}{B_9^{m_{\mathcal{J}}+k+q}}, \tag{31}$$

$$I_{22} = \begin{cases} I_{22a} & b_5 \geq b_7, x_2 \leq 0 \\ I_{22b} & b_5 < b_7, x_2 \leq 0 \\ I_{22a} - Q_2 & b_5 \geq b_7, x_2 > 0 \\ I_{22b} + Q_2 & b_5 < b_7, x_2 > 0, \end{cases} \tag{32}$$

in which $I_{22a}$, $I_{22b}$, and $Q_2$ are given as

$$I_{22a} = \frac{\left(m_1\rho_1^{-1}\right)^{m_1}\left(m_{\mathcal{J}}\rho_{\mathcal{J}}^{-1}\right)^{m_{\mathcal{J}}}e^{-B_4b_5}}{\Gamma\left(m_{\mathcal{J}}\right)\Gamma(m_1)} \times \sum_{j=0}^{m_2-1}\frac{\left(m_2\rho_2^{-1}\right)^j\Gamma(m_1+j)}{j!B_4^{m_1+j}}\sum_{l=0}^{m_1+j-1}\frac{B_4^l}{l!} \times \sum_{q=0}^{l}\binom{l}{q}b_4^q b_5^{l-q}\frac{\Gamma\left(m_{\mathcal{J}}+q\right)}{B_{10}^{m_{\mathcal{J}}+q}}, \tag{33}$$

$$I_{22b} = \frac{\left(m_1\rho_1^{-1}\right)^{m_1}\left(m_{\mathcal{J}}\rho_{\mathcal{J}}^{-1}\right)^{m_{\mathcal{J}}}e^{-B_4b_7}}{\Gamma\left(m_{\mathcal{J}}\right)\Gamma(m_1)} \times \sum_{j=0}^{m_2-1}\frac{\left(m_2\rho_2^{-1}\right)^j\Gamma(m_1+j)}{j!B_4^{m_1+j}}\sum_{l=0}^{m_1+j-1}\frac{B_4^l}{l!} \times \sum_{q=0}^{l}\binom{l}{q}b_6^q b_7^{l-q}\frac{\Gamma\left(m_{\mathcal{J}}+q\right)}{B_{11}^{m_{\mathcal{J}}+q}}, \tag{34}$$

$$Q_2 = \frac{\left(m_1\rho_1^{-1}\right)^{m_1}\left(m_{\mathcal{J}}\rho_{\mathcal{J}}^{-1}\right)^{m_{\mathcal{J}}}e^{-B_4b_5}}{\Gamma\left(m_{\mathcal{J}}\right)\Gamma(m_1)} \times \sum_{j=0}^{m_2-1}\frac{\left(m_2\rho_2^{-1}\right)^j\Gamma(m_1+j)}{j!B_4^{m_1+j}}\sum_{l=0}^{m_1+j-1}\frac{B_4^l}{l!} \times \sum_{q=0}^{l}\binom{l}{q}b_4^q b_5^{l-q}\frac{\Gamma\left(m_{\mathcal{J}}+q,B_{10}x_2\right)}{B_{10}^{m_{\mathcal{J}}+q}} - \frac{\left(m_1\rho_1^{-1}\right)^{m_1}\left(m_{\mathcal{J}}\rho_{\mathcal{J}}^{-1}\right)^{m_{\mathcal{J}}}e^{-B_4b_7}}{\Gamma\left(m_{\mathcal{J}}\right)\Gamma(m_1)} \times \sum_{j=0}^{m_2-1}\frac{\left(m_2\rho_2^{-1}\right)^j\Gamma(m_1+j)}{j!B_4^{m_1+j}}\sum_{l=0}^{m_1+j-1}\frac{B_4^l}{l!} \times \sum_{q=0}^{l}\binom{l}{q}b_6^q b_7^{l-q}\frac{\Gamma\left(m_{\mathcal{J}}+q,B_{11}x_2\right)}{B_{11}^{m_{\mathcal{J}}+q}}, \tag{35}$$

where $B_1 = m_2\rho_2^{-1} + m_1\rho_1^{-1}a_1$, $B_2 = m_{\mathcal{J}}\rho_{\mathcal{J}}^{-1} + m_1\rho_1^{-1}a_2 + B_1a_4$, $B_3 = m_{\mathcal{J}}\rho_{\mathcal{J}}^{-1} + m_1\rho_1^{-1}a_2 + B_1a_6$, $B_4 = m_2\rho_2^{-1} + m_1\rho_1^{-1}$, $B_5 = m_{\mathcal{J}}\rho_{\mathcal{J}}^{-1} + B_4a_4$, $B_6 = m_{\mathcal{J}}\rho_{\mathcal{J}}^{-1} + B_4a_6$, $B_7 = m_1\rho_1^{-1} + m_2\rho_2^{-1}b_1$, $B_8 = m_{\mathcal{J}}\rho_{\mathcal{J}}^{-1} + m_2\rho_2^{-1}b_2 + B_7b_4$, $B_9 = m_{\mathcal{J}}\rho_{\mathcal{J}}^{-1} + m_2\rho_2^{-1}b_2 + B_7b_6$, $B_{10} = m_{\mathcal{J}}\rho_{\mathcal{J}}^{-1} + B_4b_4$, $B_{11} = m_{\mathcal{J}}\rho_{\mathcal{J}}^{-1} + B_4b_6$, $x_1 = \frac{a_5-a_7}{a_6-a_4}$, $x_2 = \frac{b_5-b_7}{b_6-b_4}$. $\binom{n}{k} = \frac{n!}{k!(n-k)!}$ is the binomial coefficient. $\Gamma(m,\mu) = \int_{\mu}^{\infty}t^{m-1}e^{-\mu}dt$ and $\Gamma(m) = \int_0^{\infty}t^{m-1}e^{-t}dt$ are the upper incomplete Gamma function and Gamma function, respectively.

*Proof:* See the Appendix. ■

### B. INDIVIDUAL OUTAGE PROBABILITY

The UAV fails in decoding $\mathcal{S}_1$'s signal when either of the following three disjoint cases occurs: (i) The UAV cannot decode $\mathcal{S}_1$'s signal correctly by considering $\mathcal{S}_2$'s signal and $\mathcal{J}$'s signal as interference when $h_1 \geq h_2$; (ii) $\mathcal{S}_2$'s signal is decoded unsuccessfully by considering both signals from $\mathcal{S}_1$ and $\mathcal{J}$ as interference when $h_1 < h_2$; (iii) $\mathcal{S}_2$'s signal is decoded correctly and subtracted by SIC when $h_1 < h_2$, but the UAV is still unable to decode $\mathcal{S}_1$'s signal. Accordingly, the IOP of $\mathcal{S}_1$ can be expressed as follows:

$$p_1 = 1 - I_8 - I_2, \tag{36}$$

in which $I_8$ is calculated as

$$I_8 = \Pr\{(\gamma_1 \geq A_1)\cap(h_1 \geq h_2)\} = \begin{cases} I_{8a} & \mu_2A_1 \geq \mu_1 \\ I_{8b} & \text{otherwise,} \end{cases} \tag{37}$$

where

$$I_{8a} = \Pr\left\{h_1 \geq a_1h_2 + a_2h_{\mathcal{J}} + a_3\right\}, \tag{38}$$

$$I_{8b} = \Pr\left\{\left(h_1 \geq a_1h_2 + a_2h_{\mathcal{J}} + a_3\right)\cap(h_1 \geq h_2)\right\}, \tag{39}$$

$I_{8a}$ and $I_{8b}$ are derived in the following lemma.

*Lemma 2:* The closed-form expression of the probability $I_{8a}$ and $I_{8b}$ can be expressed as follows:

$$I_{8a} = \frac{\left(m_2\rho_2^{-1}\right)^{m_2}\left(m_{\mathcal{J}}\rho_{\mathcal{J}}^{-1}\right)^{m_{\mathcal{J}}}e^{-m_1\rho_1^{-1}a_3}}{\Gamma\left(m_{\mathcal{J}}\right)\Gamma(m_2)} \times \sum_{i=0}^{m_1-1}\frac{\left(m_1\rho_1^{-1}\right)^i}{i!}\sum_{j=0}^{i}\binom{i}{j}a_1^j\sum_{k=0}^{i-j}a_3^{i-j-k}a_2^k \times \binom{i-j}{k}\frac{\Gamma(m_2+j)}{B_1^{m_2+j}}\frac{\Gamma\left(m_{\mathcal{J}}+k\right)}{B_{12}^{m_{\mathcal{J}}+k}}, \tag{40}$$

$$I_{8b} = I_{8a} + I_{11a} - I_{10} + \frac{\left(m_2\rho_2^{-1}\right)^{m_2}\left(m_{\mathcal{J}}\rho_{\mathcal{J}}^{-1}\right)^{m_{\mathcal{J}}}e^{-B_4a_7}}{\Gamma\left(m_{\mathcal{J}}\right)\Gamma(m_2)} \times \sum_{j=0}^{m_1-1}\frac{\left(m_1\rho_1^{-1}\right)^j\Gamma(m_2+j)}{j!B_4^{m_2+j}}\sum_{l=0}^{m_2+j-1}\frac{B_4^l}{l!} \times \sum_{q=0}^{l}\binom{l}{q}a_6^q a_7^{l-q}\frac{\Gamma\left(m_{\mathcal{J}}+q\right)}{B_{13}^{m_{\mathcal{J}}+q}}, \tag{41}$$

where $B_{12} = m_{\mathcal{J}}\rho_{\mathcal{J}}^{-1} + m_1\rho_1^{-1}a_2$ and $B_{13} = m_{\mathcal{J}}\rho_{\mathcal{J}}^{-1} + B_4a_6$.

*Proof:* See the Appendix. ■

Similar to how it is calculated the IOP for $\mathcal{S}_1$, the IOP of $\mathcal{S}_2$ can be represented as

$$p_2 = 1 - I_9 - I_1, \tag{42}$$

in which $I_9$ is given as

$$I_9 = \Pr\left\{\left(\gamma_2' \geq A_2\right)\cap(h_1 < h_2)\right\} = \begin{cases} I_{9a} & \mu_1'A_2 \geq \mu_2' \\ I_{9b} & \text{otherwise,} \end{cases} \tag{43}$$

where

$$I_{9a} = \Pr\left\{h_2 \geq b_1h_1 + b_2h_{\mathcal{J}} + b_3\right\}, \tag{44}$$

$$I_{9b} = \Pr\left\{\left(h_2 \geq b_1 h_1 + b_2 h_{\mathcal{J}} + b_3\right) \cap \left(h_2 > h_1\right)\right\}, \quad (45)$$

$I_{9a}$ and $I_{9b}$ are calculated in the following lemma.

*Lemma 3:* The closed-form expression of the probability $I_9$ can be given as follows:

$$\begin{aligned} I_{9a} = & \frac{\left(m_1\rho_1^{-1}\right)^{m_1}\left(m_{\mathcal{J}}\rho_{\mathcal{J}}^{-1}\right)^{m_{\mathcal{J}}} e^{-m_2\rho_2^{-1}b_3}}{\Gamma\left(m_{\mathcal{J}}\right)\Gamma(m_1)} \\ & \times \sum_{i=0}^{m_2-1} \frac{\left(m_2\rho_2^{-1}\right)^i}{i!} \sum_{j=0}^{i} \binom{i}{j} b_1^j \sum_{k=0}^{i-j} b_3^{i-j-k} b_2^k \\ & \times \binom{i-j}{k} \frac{\Gamma(m_1+j)}{B_7^{m_1+j}} \frac{\Gamma\left(m_{\mathcal{J}}+k\right)}{B_{14}^{m_{\mathcal{J}}+k}}, \end{aligned} \quad (46)$$

$$\begin{aligned} I_{9b} = & I_{9a} + I_{21a} - I_{20} \\ & + \frac{\left(m_1\rho_1^{-1}\right)^{m_1}\left(m_{\mathcal{J}}\rho_{\mathcal{J}}^{-1}\right)^{m_{\mathcal{J}}} e^{-B_4 b_7}}{\Gamma\left(m_{\mathcal{J}}\right)\Gamma(m_1)} \\ & \times \sum_{j=0}^{m_2-1} \frac{\left(m_2\rho_2^{-1}\right)^j \Gamma(m_1+j)}{j! B_4^{m_1+j}} \sum_{l=0}^{m_1+j-1} \frac{B_4^l}{l!} \\ & \times \sum_{q=0}^{l} \binom{l}{q} b_6^q b_7^{l-q} \frac{\Gamma\left(m_{\mathcal{J}}+q\right)}{B_{15}^{m_{\mathcal{J}}+q}}, \end{aligned} \quad (47)$$

where $B_{14} = m_{\mathcal{J}}\rho_{\mathcal{J}}^{-1} + m_2\rho_2^{-1}b_2$ and $B_{15} = m_{\mathcal{J}}\rho_{\mathcal{J}}^{-1} + B_4 b_6$.

*Proof:* See the Appendix. ■

## IV. JOINT POWER ALLOCATION AND UAV PLACEMENT DESIGN

In this section, a joint power allocation and UAV placement design are interpreted for both scenarios of the fixed and mobile jammers. Then, a competition game involving two players, the UAV and the smart jammer, is formulated. Eventually, the complexities of the proposed algorithms are analyzed.

Theoretically, accurate calculation of the power allocation and UAV placement can be done when having obtained the OOP as follows: (i) find the roots of the first differentiation of the OOP, (ii) compare between the limit points and the obtained roots to find the final solution. However, due to the complexity of the OOP, closed-form expressions of the first differentiation of the OOP and its roots are infeasible to obtain. Another way to find the discretized optimal power allocation and UAV placement is by performing exhaustive search [50], i.e., calculating all possible solutions in terms of the power allocation and UAV placement to find the optimal ones. However, this search takes a long time. Thus, in this work we propose a set of hybrid SA-greedy algorithms.

Further, it has been shown that the power consumption of wireless communication and of hovering is much smaller compared to the power consumption of the UAV moving [51], [52]. Hence, to decrease the power consumption, the UAV should find the optimal placement fast and go there directly. Otherwise, in the case of being jammed, if the UAV uses mobility, i.e., moving along following the jammer, to control the situation, the jammer can adopt a tactic of just running around to drain the UAV's power.

### A. SCENARIO I: FIXED JAMMER

In this scenario, the jammer location is fixed, e.g., any interferer working at the same frequency band with the legal system can be considered as a jammer. If the UAV detects a jamming attack from a malicious jammer and then also estimates the jammer's location, e.g., using a method proposed in [38], [53], [54], it has the capability to move to an optimal position combining with optimal power allocation to mitigate the effects of jamming attacks. It is noticed that the main objective of the UAV is to provide the required communication reliability. In this situation, the optimization problem is formulated based on the OOP in (9) as follows:

$$\begin{aligned} P_I = \min_{\mu_1, \mu_1', x_u, y_u} \quad & p\left(\mu_1, \mu_1', x_u, y_u\right) && \text{(48a)} \\ \text{subject to:} \quad & 0 < \mu_1 < 1 && \text{(48b)} \\ & 0 < \mu_1' < 1 && \text{(48c)} \\ & x_{umin} \leq x_u \leq x_{umax} && \text{(48d)} \\ & y_{umin} \leq y_u \leq y_{umax} && \text{(48e)} \end{aligned}$$

in which both constraints of (48b) and (48c) are related to the power allocation factors as mentioned in Section II. The constraints of (48d) and (48e) are for the location of the UAV with fixed altitudes. This is because the UAV is only allowed to move inside of the legal area and therefore $x_{umin}$, $x_{umax}$, $y_{umin}$, and $y_{umax}$ are determined based on the border. Note that $x_{\mathcal{J}}$ and $y_{\mathcal{J}}$ are fixed and outside of the border.

Due to the fact that the OOP function is a complex function with many input parameters as presented in Section III, it is very complex to find the exact solution for the optimal values of power allocation and UAV placement minimizing the OOP. Moreover, parameters such as path-loss exponents and shapes $m_i$ and $m_{\mathcal{J}}$ between the UAV and other nodes can change following the location of each node. On the other hand, meta-heuristics can provide appropriate methods to find the best solution within the time constraints. Therefore, we propose an algorithm using a hybrid SA-Greedy to find the optimal power allocation and UAV placement. In [55], the author shows that the global minimum can be obtained with the SA method by changing temperature parameter and cooling schedule to break out of the local minimum. However, the SA method can take a huge number of iterations for convergence. On the other hand, the Greedy method can reach the local minimum faster when the initial solution is close to the local minimum [55]. Therefore, we propose a hybrid SA-Greedy algorithm following two steps: (i) The SA method is used first for searching for the global minimum. The number of iterations can be reduced significantly when the obtained results have a light fluctuation around the global minimum; and (ii) The Greedy method is then employed to find the final global minimum. The main idea

of the Greedy method is that the algorithm finds the direction of the steepest descent at each step to go until reaching the local minimum to minimize the cost function, i.e., the OOP function in (9). This means that the Greedy algorithm needs to determine the neighbors of the current position at each step to evaluate the cost function for each neighbor and then decide which direction to go next. A pseudo-code of the hybrid SA-Greedy algorithm is provided in Algorithm 1. In general, this function requires $k$ input parameters, maximum number of iterations $N$, maximum temperature $T$, and factor $\epsilon$, while the output parameters include $j$ elements. At the first step, the SA method is used. First, the initial point and neighbor are chosen randomly. The new solution $S'$ is accepted immediately if its cost function is smaller than the cost function of the current solution as shown in the 9th line. However, when the cost function of $S'$ is still bigger than that for $S$, the new solution can still be accepted with a probability of accepting to escape the local minimum as shown in the lines 12 and 13. An important parameter here is the temperature $T$ in which the probability of accepting worse moves goes up at high temperatures, while this probability is small at low temperature. Moreover, a trade-off between the quality of the attained solutions and speed of convergence related to updating temperature as shown in the 17th line via $\epsilon$ is necessary to consider, i.e., if the temperature decreases fast, worse solutions are found with a smaller computation time. Here, the stop condition is based on a predetermined number of iterations $N$ under the constraint of without improvement of the best found solution [56]. In the second step, a Greedy method is adopted. Different to the SA method, the new solutions $S'$ include all closest neighbors of the current solution. Then all new solutions are evaluated by the cost function and the best solution is decided in the 23th line. If there is no better solution than the current solution, the Greedy method stops. Note that all output parameters are updated when a new solution is accepted as shown in the lines 10, 14, and 24. Finally, all output parameters are returned under the name of function.

**Algorithm 1** The Hybrid SA-Greedy Algorithm in Pseudo-Code

1: **function** $[output_j]$ = Name_Function($input_k, N, T, \epsilon$):
2: **Step1:SimulatedAnnealingmethod**
3: Generation of the initial solution $S = S_0$;
4: Calculate the cost function at $S$: $f(S)$;
5: **for** i = 1:$N$ **do**
6: Generate a random neighbor $S'$;
7: Calculate the cost function at $S'$: $f(S')$;
8: Calculate $\Delta = f(S') - f(S)$;
9: **if** $\Delta \leq 0$ **then**
10: $S = S'$; Update $[output_j]$;
11: **else**
12: Calculate the probability of accepting a non-improving neighbor: $\delta = e^{-\frac{\Delta}{T}}$;
13: **if** $\delta >$ random[0,1) **then**
14: $S = S'$; Update $[output_j]$;
15: **end if**
16: **end if**
17: Update temperature: $T = \epsilon T$;
18: **end for**
19: **Step2:Greedymethod**
20: **while** True **do**
21: Update $S'$ is all closest neighbors of $S$;
22: Calculate the cost function $f(S')$;
23: **if** $f(S') < f(S)$ **then**
24: $S = S'$; Update $[output_j]$;
25: **else**
26: **Break**;
27: **end if**
28: **end while**
29: return $[output_j]$;
30: **end function**

In this work, we consider two power allocation strategies: (i) Firstly, the power levels for the two source nodes are different for both states of the dynamic decoding order (DDO), i.e., $(\mu_1, \mu_2) \neq (\mu_1', \mu_2')$. In other words, two pairs of power allocation factors are used for both states of the DDO; and (ii) Secondly, the power level of the weaker source node is always larger than the stronger one for both states of the DDO. This case uses only one pair of power allocation factors with $\mu_1 = \mu_2'$. To minimize the OOP at the specific locations of both jammer and UAV, we formulate the optimization problem as in (49) to find the optimal power allocation. Note that for the given optimization problems in (48) and (49) there always exist the maximum and minimum points as shown in the remark 1. Accordingly, by applying Algorithm 1, the function finding optimal power allocation is provided in Table 1, namely *PowerAllocation_SAG*. Here, input parameters of power allocation are $\mu_1 \longleftarrow [\mu_{1min}{:}\mu_{1max}]$, $\mu_1' \longleftarrow [\mu_{1min}' : \mu_{1max}']$.

$$O_1 = \min_{\mu_1, \mu_1'} \quad p(\mu_1, \mu_1') \tag{49a}$$

$$\text{subject to:} \quad 0 < \mu_1 < 1 \tag{49b}$$

$$0 < \mu_1' < 1. \tag{49c}$$

*Remark 1:* The OOP in (9) as a function of the power allocation, UAV placement, and jammer location always has at least one maximum point and one minimum point over its domains.

*Proof:* As provided above, a range on the power allocation for each source, UAV location, and jammer placement are defined. Moreover, as presented in Section III, we can see that $p$ is a continuous function on its respective domains. Following the extreme value theorem [57], this remark is proved. ■

To solve the optimization problem in (48), a function finding optimal power allocation and UAV placement is provided by applying the proposed hybrid SA-Greedy algorithm as shown in Table 1, namely

**TABLE 1.** The functions finding the optimal power allocation and/or uav placement or jammer placement.

| **Function name** | *PowerAllocation_SAG* | *PowerAllocation_UAV Placement_SI_SAG* | *Jammer_Placement_SI_SAG* | *Jammer_Placement _SII_SAG* | *PowerAllocation_UAV Placement_SII_SAG* |
|---|---|---|---|---|---|
| **Input paramters** | $h,\ x_u,\ y_u,\ x_{\mathcal{J}},\ y_{\mathcal{J}},\ x_i,\ y_i,\ R_{1th},\ R_{2th},\ \zeta_1,\ \zeta_2,\ \zeta_{\mathcal{J}},\ P,\ P_{\mathcal{J}},\ \sigma_0^2,\ \sigma_1^2,\ \sigma_2^2,\ W,\ m_1,\ m_2,\ m_{\mathcal{J}},\ \mu_1,\ \mu_1^{'},\ N_1,\ T_1,\ \epsilon_1$ | $h,\ x_{\mathcal{J}},\ y_{\mathcal{J}},\ x_i,\ y_i,\ R_{1th},\ R_{2th},\ \zeta_1,\ \zeta_2,\ \zeta_{\mathcal{J}},\ P,\ P_{\mathcal{J}},\ \sigma_0^2,\ \sigma_1^2,\ \sigma_2^2, W, m_1, m_2, m_{\mathcal{J}},\ \mu_1,\ \mu_1^{'},\ x_u,\ y_u,\ N_2,\ T_2,\ \epsilon_2$ | $h,\ x_i,\ y_i,\ x_u,\ y_u,\ R_{1th},\ R_{2th},\ \zeta_1,\ \zeta_2,\ \zeta_{\mathcal{J}},\ P,\ P_{\mathcal{J}},\ \sigma_0^2,\ \sigma_1^2,\ \sigma_2^2,\ W,\ m_1,\ m_2,\ m_{\mathcal{J}},\ \mu_1,\ \mu_1^{'},\ x_{\mathcal{J}},\ y_{\mathcal{J}},\ N_3,\ T_3,\ \epsilon_3$ | $h,\ x_u,\ y_u,\ x_i,\ y_i,\ R_{1th},\ R_{2th},\ \zeta_1,\ \zeta_2,\ \zeta_{\mathcal{J}},\ P,\ P_{\mathcal{J}},\ \sigma_0^2,\ \sigma_1^2,\ \sigma_2^2, W, m_1, m_2, m_{\mathcal{J}},\ \mu_1,\ \mu_1^{'},\ x_{\mathcal{J}},\ y_{\mathcal{J}},\ N_4,\ T_4,\ \epsilon_4$ | $h, x_i, y_i, R_{1th}, R_{2th}, \zeta_1, \zeta_2, \zeta_{\mathcal{J}}, P, P_{\mathcal{J}}, \sigma_0^2, \sigma_1^2, \sigma_2^2, W, m_1, m_2, m_{\mathcal{J}}, \mu_1, \mu_1^{'}, x_{\mathcal{J}}, y_{\mathcal{J}}, x_u, y_u, N_5, T_5, \epsilon_5$ |
| **Output paramters** | $\left(\mu_{1opt}, \mu_{1opt}^{'}, p_{opt}\right)$ | $\left(\begin{matrix}\mu_{1opt}, \mu_{1opt}^{'},\\ x_{uopt}, y_{uopt}, p_{opt}\end{matrix}\right)$ | $\left(x_{\mathcal{J}opt}, y_{\mathcal{J}opt}, p_{opt}\right)$ | $\left(\begin{matrix}\mu_{1opt}, \mu_{1opt}^{'},\\ x_{\mathcal{J}opt}, y_{\mathcal{J}opt}, p_{opt}\end{matrix}\right)$ | $\left(\begin{matrix}\mu_{1opt}, \mu_{1opt}^{'}, x_{uopt},\\ y_{uopt}, p_{opt}\end{matrix}\right)$ |
| **Cost function** | The OOP in (9) | The OOP in (9) | $f = 1 - p_{opt}$ where $p_{opt}$ is obtained by running the *PowerAllocation_UAV Placement_SI_SAG* function | $f = 1 - p_{opt}$ where $p_{opt}$ is obtained by running the *PowerAllocation_SAG* function | $f = p_{opt}$ where $p_{opt}$ is obtained by running the *Jammer_Placement _SII_SAG* function |
| **Solution** $S$ | $\left(\mu_1, \mu_1^{'}\right)$ | $\left(\mu_1, \mu_1^{'}, x_u, y_u\right)$ | $\left(x_{\mathcal{J}}, y_{\mathcal{J}}\right)$ | $\left(x_{\mathcal{J}}, y_{\mathcal{J}}\right)$ | $\left(\mu_1, \mu_1^{'}, x_u, y_u\right)$ |

**TABLE 2.** The reactions of both players for the non-cooperative game in the first scenario.

| **Fixed location of the smart jammer** | **Optimal power allocation and UAV placement** | **Optimal OOP** |
|---|---|---|
| $(x_{\mathcal{J}.1}, y_{\mathcal{J}.1})$ | $\left(\mu_{1opt.1}, \mu_{1opt.1}^{'}, x_{uopt.1}, y_{uopt.1}\right)$ | $p_{uopt.1}$ |
| $(x_{\mathcal{J}.2}, y_{\mathcal{J}.2})$ | $\left(\mu_{1opt.2}, \mu_{1opt.2}^{'}, x_{uopt.2}, y_{uopt.2}\right)$ | $p_{uopt.2}$ |
| ... | ... | ... |
| $(x_{\mathcal{J}.k}, y_{\mathcal{J}.k})$ | $\left(\mu_{1opt.k}, \mu_{1opt.k}^{'}, x_{uopt.k}, y_{uopt.k}\right)$ | $p_{uopt.k}$ |
| ... | ... | ... |
| $(x_{\mathcal{J}.\omega}, y_{\mathcal{J}.\omega})$ | $\left(\mu_{1opt.\omega}, \mu_{1opt.\omega}^{'}, x_{uopt.\omega}, y_{uopt.\omega}\right)$ | $p_{uopt.\omega}$ |
| **The UAV can change its location and power allocation for the two source nodes, it thus can always find the best solution to minimize the OOP** | | |
| **The smart jammer aims to stay at fixed placement offering the highest effectiveness of attacking. The best solution for the smart jammer is determined as follows:** $\left(x_{\mathcal{J}opt}, y_{\mathcal{J}opt}\right) \leftarrow p_{\mathcal{J}opt} = \max\left(p_{uopt.1}, p_{uopt.2}, ..., p_{uopt.\omega}\right)$ | | |

*PowerAllocation_UAVPlacement_SI_SAG*. Here, input parameters of power allocation and UAV placement are $\mu_1 \longleftarrow [\mu_{1min} : \mu_{1max}]$, $\mu_1' \longleftarrow [\mu_{1min}' : \mu_{1max}']$, $x_u \longleftarrow [x_{umin} : x_{umax}]$, $y_u \longleftarrow [y_{umin} : y_{umax}]$. It is noted that the number of iterations $N_1$ and $N_2$ play an important role deciding on the quality of the final results.

When the jammer is smarter but its location is still fixed, the jammer knows both sources' positions and the UAV's strategies (power allocation and placement) maximizing the communication reliability. The reactions of both UAV and smart jammer are provided in Table 2. Accordingly, the UAV can move freely and thus find the best strategies minimizing the OOP regardless of the position of the smart jammer. In contrast, the jammer aims to save the power consumption while the power consumption for both movement and finding optimal position is much more than for communication. Therefore, the best strategy for the smart jammer is to find a placement so that the reliability of the legitimate wireless communication system is the most degraded compared to other positions and then stay at this fixed location. Of course, the smart jammer understands regardless of its placement, the UAV can always find the best solution to defend against the jamming attack, i.e., minimizing the OOP. As presented in Table 2, both UAV and smart jammer find the best solutions for them and then keep staying at their fixed solutions as the equilibrium point. Finally, we can realize that the benefits of both UAV and smart jammer are in conflict. Consequently, we model the interactions between the UAV and smart jammer as a two-player non-cooperative game as follows [58]:

$$\mathcal{G} = \{\mathcal{N}, \mathcal{S}, \mathcal{U}\}, \tag{50}$$

where $\mathcal{N} = \{\mathcal{J}, \text{UAV}\}$ is the set of game players including the smart jammer and UAV. $\mathcal{S}$ is the strategy set, $\mathcal{S} = \mathcal{S}_{\mathcal{J}} \times \mathcal{S}_u$, where $\mathcal{S}_{\mathcal{J}}$ and $\mathcal{S}_u$ are the sets of strategies of the smart jammer and UAV, respectively. $\mathcal{U}$ is the utility set, $\mathcal{U} = (\mathcal{U}_{\mathcal{J}}, \mathcal{U}_u)$, where $\mathcal{U}_{\mathcal{J}}$ and $\mathcal{U}_u$ are the utility functions of the jammer and UAV, respectively.

For the UAV, both power allocation and placement are taken into account to maximize the communication reliability with each jammer position as shown in (48). Contrarily, the smart jammer only considers its position to maximize the OOP when the UAV can always find the best solution. Therefore, $(x_{\mathcal{J}}, y_{\mathcal{J}})$ and $(x_u, y_u, \mu_1, \mu_1')$ represent the strategies for the smart jammer and UAV, respectively. Then, $\mathcal{S}_{\mathcal{J}}$ and $\mathcal{S}_u$ can be determined as the set of all the possible strategies $(x_{\mathcal{J}}, y_{\mathcal{J}})$ and $(x_u, y_u, \mu_1, \mu_1')$, respectively. Here, the UAV has to check the smart jammer location every time. Once the UAV detects any movement of jammer, it needs to find the optimal power allocation and placement before going there to minimize the OOP. As presented previously, both UAV and smart jammer aim to satisfy their own requirements, in which the UAV wants to minimize the OOP using both power allocation and its placement strategies, whereas the smart jammer aims to maximize the OOP using its location strategy, therefore the utility functions $\mathcal{U}_{\mathcal{J}}$ and $\mathcal{U}_u$ can be defined as follows:

$$\begin{cases} \mathcal{U}_{\mathcal{J}} = +p\left(x_{\mathcal{J}}, y_{\mathcal{J}}\right) \\ \mathcal{U}_u = -p\left(\mu_1, \mu_1', x_u, y_u\right) \end{cases} \tag{51}$$

where $p$ is the OOP in (9). The UAV problem is already formulated as in (48). Furthermore, the problem for the smart jammer can be formulated as in (52). Following

the remark 1, the maximum point of the problem in (52) exists. Accordingly, the equilibrium point for the non-cooperative game is found when both players have satisfied their own requirements. This means that both (48) and (52) happen together as shown in the following theorem. Thereafter, applying the proposed hybrid SA-Greedy algorithm, a function finding optimal jammer location is presented in Table 1, namely *Jammer_Placement_SI_SAG*. Here, the input paramters of the power allocation, UAV placement, and jammer location are $\mu_1 \longleftarrow [\mu_{1min} : \mu_{1max}]$, $\mu_1' \longleftarrow [\mu'_{1min} : \mu'_{1max}]$, $x_{\mathcal{J}} \longleftarrow [x_{\mathcal{J}min} : x_{\mathcal{J}max}]$, $y_{\mathcal{J}} \longleftarrow [y_{\mathcal{J}min} : y_{\mathcal{J}max}]$, $x_u \longleftarrow [x_{umin} : x_{umax}]$, $y_u \longleftarrow [y_{umin} : y_{umax}]$. Note that the smart jammer's location is fixed, thus the UAV can easily find the optimal power allocation and placement as presented above.

$$P_{\mathcal{J}} = \max \mathcal{U}_{\mathcal{J}} = \max_{x_{\mathcal{J}}, y_{\mathcal{J}}} \; P_I \tag{52a}$$

$$\text{subject to:} \quad x_{\mathcal{J}min} \le x_{\mathcal{J}} \le x_{\mathcal{J}max} \tag{52b}$$

$$y_{\mathcal{J}min} \le y_{\mathcal{J}} \le y_{\mathcal{J}max} \tag{52c}$$

*Theorem 1:* There exists the Nash equilibrium point for the non-cooperative game $\mathcal{G}$ in (50).

*Proof:* In fact, the game $\mathcal{G}$ in (50) is a finite game with the two players including the UAV and smart jammer as well as finite strategies for each player as mentioned above. Therefore, a mixed-strategy Nash equilibrium exists [59, Proposition 33.1]. Then this theorem is obtained. ■

### B. SCENARIO II: MOBILE JAMMER

Let us consider that the jammer is mobile and smarter. In other words, the jammer can know the location of both source nodes and UAV as well as the UAV's strategies to minimize the OOP. This can help the smart jammer find an optimal location in terms of maximizing the OOP. When the power budget of the jammer can cover for all communication, computation, and movement, the smart jammer can always find the optimal placement and move there to generate the jamming signal with the highest effectiveness to defeat the legitimate system, i.e., the OOP is maximized. This is the best strategy for the smart jammer. If the UAV keeps staying at the fixed location, the smart jammer is also located at the fixed optimal placement. In fact, the smart jammer is always active to attack the UAV, while the UAV does not know where the smart jammer is and when it attacks. This means that when the UAV detects the jammer location, the UAV also can find a new optimal power allocation and location and then goes directly there. However, the smart jammer also can adapt to new optimal position to defeat the UAV communication. In the worst case, the UAV will always be attacked by the smart jammer reaching immediately to its optimal position. If the UAV keeps balance and moves to the new optimal placement whenever it detects a responding optimal location of the smart jammer, it would consume a lot of power for the movement and computation [51], while the achievable communication reliability can even be worse than the previous placement.

**TABLE 3.** The reactions of both players for the competition game in the second scenario.

| Fixed power allocation and UAV placement | Optimal jammer position | Optimal OOP |
|---|---|---|
| $\left(\mu_{1opt.1}, \mu'_{1opt.1}, x_{u.1}, y_{u.1}\right)$ | $\left(x_{\mathcal{J}opt.1}, y_{\mathcal{J}opt.1}\right)$ | $p_{\mathcal{J}opt.1}$ |
| $\left(\mu_{1opt.2}, \mu'_{1opt.2}, x_{u.2}, y_{u.2}\right)$ | $\left(x_{\mathcal{J}opt.2}, y_{\mathcal{J}opt.2}\right)$ | $p_{\mathcal{J}opt.2}$ |
| ... | ... | ... |
| $\left(\mu_{1opt.k}, \mu'_{1opt.k}, x_{u.k}, y_{u.k}\right)$ | $\left(x_{\mathcal{J}opt.k}, y_{\mathcal{J}opt.k}\right)$ | $p_{\mathcal{J}opt.k}$ |
| ... | ... | ... |
| $\left(\mu_{1opt.\vartheta}, \mu'_{1opt.\vartheta}, x_{u.\vartheta}, y_{u.\vartheta}\right)$ | $\left(x_{\mathcal{J}opt.\vartheta}, y_{\mathcal{J}opt.\vartheta}\right)$ | $p_{\mathcal{J}opt.\vartheta}$ |
| **The jammer accepts mobility and then it can always find the best position as the best solution maximizing the OOP** | | |
| **The UAV wants to stay at fixed position with optimal power allocation, where the effectiveness of attacking is the lowest. The best solution for the UAV is defined as follows:** | | |
| $\left(\begin{matrix}\mu_{1opt}, \mu'_{1opt},\\ x_{uopt}, y_{uopt}\end{matrix}\right) \leftarrow p_{uopt} = \min\left(p_{\mathcal{J}opt.1}, p_{\mathcal{J}opt.2}, ..., p_{\mathcal{J}opt.\vartheta}\right)$ | | |

To react to this situation, the UAV should select a placement offering the best communication reliability compared to other possible positions and stay at this fixed location without monitoring the jammer placement. This is also to save power for the UAV. The reactions of both the smart jammer and the UAV are illustrated in Table 3. Accordingly, the UAV and smart jammer obtain their objectives together at their fixed best solutions as the equilibrium point. With this scenario, we model the interactions between the UAV and smart jammer as a two-player non-cooperative game as in (50).

With this model, the smart jammer only takes its position into account to attack the legal system and disrupt the ongoing transmissions. In contrast, the UAV has to consider both power allocation and its placement to maximize the communication reliability in terms of minimizing the OOP under the constraint of the optimal smart jammer placement. As a result, $(x_{\mathcal{J}}, y_{\mathcal{J}})$ and $(x_u, y_u, \mu_1, \mu_1')$ represent the strategies for the smart jammer and UAV, respectively. Then, $\mathcal{S}_{\mathcal{J}}$ and $\mathcal{S}_u$ can be determined as the set of all the possible strategies $(x_{\mathcal{J}}, y_{\mathcal{J}})$ and $(x_u, y_u, \mu_1, \mu_1')$, respectively. To save the power consumption for moving, the smart jammer always checks the UAV placement when it reached the optimal position. The smart jammer only moves to the new optimal location once it detects a movement of the UAV and the new optimal position is better than the current one in terms of maximizing the OOP. In contrast, the UAV understands that no matter where it locates it can be attacked by the smart jammer staying at optimal position. Therefore, both UAV and smart jammer try to find best solutions satisfying their own requirements as mentioned above. Accordingly, the jammer aims to maximize the OOP, while the UAV wants to minimize the OOP, therefore the utility functions $\mathcal{U}_{\mathcal{J}}$ and $\mathcal{U}_u$ can be defined as follows:

$$\begin{cases} \mathcal{U}_{\mathcal{J}} = +p\left(x_{\mathcal{J}}, y_{\mathcal{J}} | \mu_{1opt}, \mu'_{1opt}\right) \\ \mathcal{U}_u = -p\left(\mu_1, \mu_1', x_u, y_u\right) \end{cases} \tag{53}$$

where $p$ is the OOP in (9). Due to the fact that the UAV finds the optimal power allocation at each position, the problem for the smart jammer is presented as in (54). Then the problem for the UAV can be formulated as in (55). The equilibrium point is found when both players satisfied their own requirements. This means that both (54) and (55) happen together as shown in Theorem 1. Accordingly, a function finding optimal jammer position is proposed using the proposed hybrid SA-Greedy algorithm as illustrated in Table 1, namely *Jammer_Placement_SII_SAG*. With this function, the input parameters of power allocation and jammer location are $\mu_1 \longleftarrow [\mu_{1min} : \mu_{1max}]$, $\mu_1' \longleftarrow [\mu_{1min}' : \mu_{1max}']$, $x_{\mathcal{J}} \longleftarrow [x_{\mathcal{J}min} : x_{\mathcal{J}max}]$, $y_{\mathcal{J}} \longleftarrow [y_{\mathcal{J}min} : y_{\mathcal{J}max}]$. Then, another function is proposed to find the optimal power allocation and UAV placement using the proposed hybrid SA-Greedy algorithm as shown in Table 1, namely *PowerAllocation_UAVPlacement_SII_SAG*. Here, the input parameters of the power allocation, UAV location, and jammer position are $\mu_1 \longleftarrow [\mu_{1min} : \mu_{1max}]$, $\mu_1' \longleftarrow [\mu_{1min}' : \mu_{1max}']$, $x_{\mathcal{J}} \longleftarrow [x_{\mathcal{J}min} : x_{\mathcal{J}max}]$, $y_{\mathcal{J}} \longleftarrow [y_{\mathcal{J}min} : y_{\mathcal{J}max}]$, $x_u \longleftarrow [x_{umin} : x_{umax}]$, $y_u \longleftarrow [y_{umin} : y_{umax}]$.

$$O_2 = \max \mathcal{U}_{\mathcal{J}} = \max_{x_{\mathcal{J}}, y_{\mathcal{J}}} \; O_1 \tag{54a}$$

$$\text{subject to:} \quad x_{\mathcal{J}min} \le x_{\mathcal{J}} \le x_{\mathcal{J}max} \tag{54b}$$

$$y_{\mathcal{J}min} \le y_{\mathcal{J}} \le y_{\mathcal{J}max} \tag{54c}$$

$$P_{II} = \min \mathcal{U}_u = \min_{x_u, y_u} \; O_2 \tag{55a}$$

$$\text{subject to:} \quad x_{umin} \le x_u \le x_{umax} \tag{55b}$$

$$y_{umin} \le y_u \le y_{umax}. \tag{55c}$$

### C. COMPLEXITY OF THE PROPOSED ALGORITHMS

For all proposed algorithms described above, the number of iterations decides the convergence of the SA method as well as the quality of the obtained solutions. However, increasing the number of iterations leads to a growth of execution time, i.e., possibly violating timing constraints in specific applications. If the number of iterations is high enough, the achievable solution is significantly close to the final global solution. This can reduce the number of iterations of the Greedy method used in the second phase. In contrast, the obtained solution fluctuates significantly around the final solution if fewer iterations were done in the SA method. As a result, the Greedy method takes more iterations to find the final solution. In addition, if the number of iterations for the SA algorithm is small, the obtained solution of the hybrid SA-Greedy algorithm may not be the global minimum. Therefore, the number of iterations for the SA method should be low enough to satisfy that the obtained solution has only light fluctuation around the global minimum. However, due to the fact that both source nodes' locations are fixed, the UAV can run all proposed algorithms once for both scenarios mentioned above to get the global solution with fixed optimal power allocation and placement.

To guarantee that all transmitted messages can reach the destinations before the deadline and while meeting the communication reliability requirement, a threshold of the OOP is needed, e.g., $p \le 10^{-5}$. The value of threshold OOP depends on each specific application [8]. Therefore, there are few possible cases in practice that need to be considered as follows:

- When the equilibrium points for both aforementioned scenarios are obtained, the OOPs are minimum. However, if these values are still higher than the given threshold OOPs, other techniques such as retransmission, relaying strategies, etc. should be used additionally to meet the communication reliability requirements and then formulate the competition game with the same approach. This is beyond the scope of this work and we leave it for future work.
- For the proposed communication protocols described in II, the achievable OOPs satisfy the communication reliability requirement. Accordingly, we can solve the non-cooperative game following two ways. First, the UAV only need to find a set of strategies (power allocation and placement) ensuring $p \le p_{threshold}$. In such a situation, there may be many equilibrium points and it can take shorter time to find the final satisfactory solution. Thus, the first sub-case may be attained online with mobile source nodes. Second, the UAV tries using best effort for finding the best strategies minimizing the OOP as we do in this work. We can see that the obtained OOP in this sub-case is better than that for the first sub-case or at least equal to the achievable OOP in the first sub-case.

## V. NUMERICAL RESULTS AND DISCUSSIONS

In this section we present numerical results for both OOP and IOP of the considered system and then investigate the effect of some parameters on them. The following system parameters are used: $W = 1$ Hz, $P = 1$W, $P_{\mathcal{J}} = 1$W, $h = 20$, $\zeta_1 = \zeta_2 = \zeta_{\mathcal{J}} = 2$, $R_{1th} = 0.1$ bps, $R_{2th} = 0.1$ bps, $\sigma_1^2 = 1e-4$, $\sigma_2^2 = 1e-4$, and $\sigma_0^2 = 10^{-10}$W/Hz [60], [61]. To reduce the number of iterations for the proposed algorithms, we setup $T_1 = T_2 = T_3 = T_4 = T_5 = 1e-3$, $\epsilon_1 = \epsilon_2 = \epsilon_3 = \epsilon_4 = \epsilon_5 = 0.9$ from experiment. As introduced in Section II, both the source nodes and the UAV are only allowed to be located in the isolated area, while the jammer can only be located outside of the border. We setup the border in which $(100 \le x_{\mathcal{J}}, -\infty < y_{\mathcal{J}} < +\infty)$ is for the smart jammer and the remainder is for the UAV and two source nodes. To check the correctness of the analysis in Section III, we also conduct computer simulations using MATLAB. In particular, for each considered OOP and IOP we first generate $10^5$ samples of the channel gains following a Gamma distribution and then check the outage conditions as defined in (9), (36), and (42). The simulation results of the OOP and IOPs are then attained by taking the average of all outage events across $10^5$ samples. We conclude the

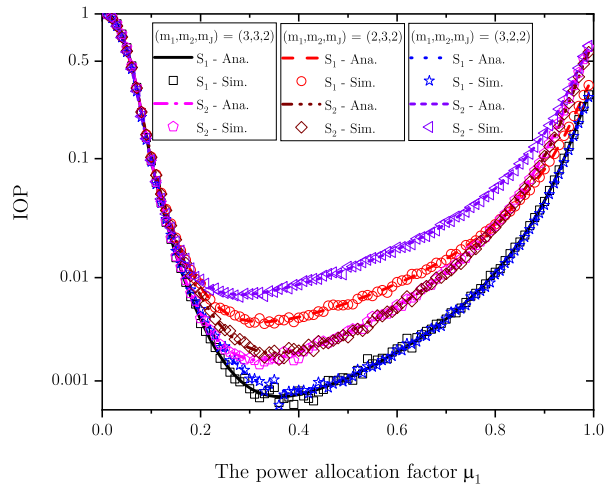


**FIGURE 3.** The validation of the calculations of the IOPs in different environments $(m_1, m_2, m_{\mathcal{J}})$.

section by discussing the impact of different parameters on the OOP.

### A. INDIVIDUAL OUTAGE PROBABILITY

Fig. 3 depicts how the IOP of $\mathcal{S}_i$ is affected by the power allocation factor with different shapes $(m_1, m_2, m_{\mathcal{J}})$ using the power allocation strategy of $\mu_1 = \mu_2'$, $(x_{\mathcal{S}_1}, y_{\mathcal{S}_1}) = (-100, 0)$, $(x_{\mathcal{S}_2}, y_{\mathcal{S}_2}) = (100, 0)$, $(x_{\mathcal{J}}, y_{\mathcal{J}}) = (150, 0)$, and $(x_u, y_u) = (-10, 0)$. Here, while the jammer is situated quite far away from the border, the UAV is located around the middle point between the two source nodes where the DDO happens with higher probability [16]. We can see that the analytical results and the simulation match very well corroborating the accuracy of the calculation. It can also be seen from the figure that the power allocation factor significantly affects the IOP for both source nodes. Moreover, when the two source nodes experience a better environment with $m_1 = m_2 = 3$, the IOPs can reduce significantly.

The effects of the jammer location on both IOPs of both source nodes are described in Fig. 4 with $m_1 = m_2 = m_{\mathcal{J}} = 3$, $\mu_1 = \mu_2' = 0.15$, $(x_{\mathcal{S}_2}, y_{\mathcal{S}_2}) = (100, 0)$, and $(x_u, y_u) = (10, 0)$. Generally, we can see that both IOPs decrease significantly with an increase of the distance between the UAV and malicious jammer due to the higher path-loss. Moreover, the first source node gains more communication reliability than the other one. This can be explained by the fact that the second source node is located at the border and thus experiences the higher path-loss. In addition, the IOPs of both source nodes go up dramatically when both source nodes stay toward close to the border. The reason is that the distances between both source nodes and UAV grow significantly.

Fig. 5 presents how the UAV placement affects the IOPs of both source nodes with $m_1 = m_2 = m_{\mathcal{J}} = 3$, $\mu_1 = \mu_2' = 0.15$, $(x_{\mathcal{S}_2}, y_{\mathcal{S}_2}) = (100, 0)$, and $(x_{\mathcal{J}}, y_{\mathcal{J}}) = (150, 0)$. It can be seen from the Figures 5a and b that both IOPs go

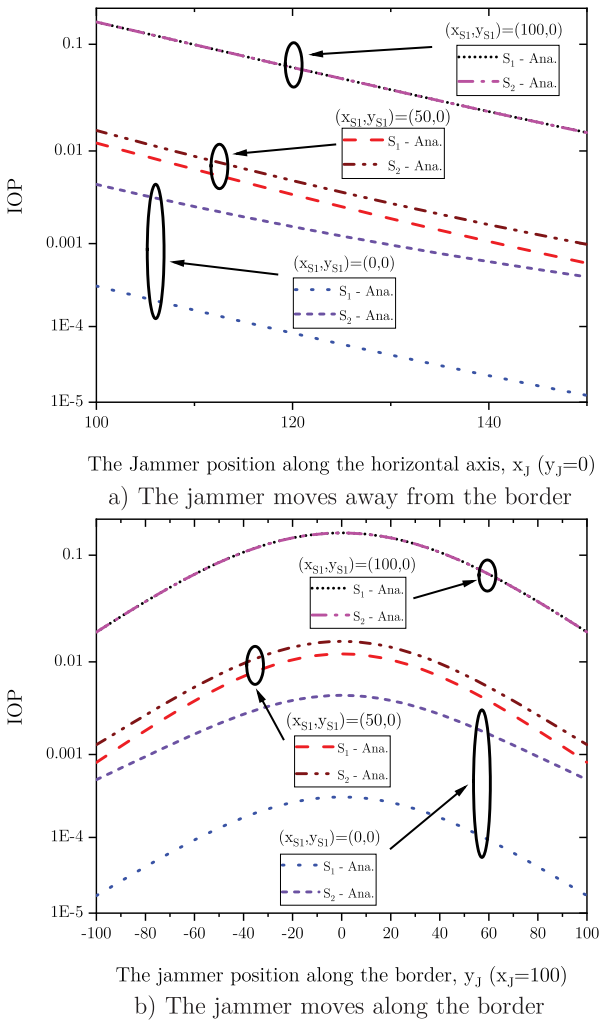


**FIGURE 4.** The effect of the jammer location on the IOPs.

down significantly when the UAV stays around on top of the source node locating far away from the border. This is because the path-loss between the UAV and this source node decreases dramatically and then more power is allocated to the source node locating at the border to overcome the higher path-loss. This result is suitable to the best UAV placement from the experiment in [40]. Furthermore, when the UAV moves toward to the border, the communication reliability between both source nodes and UAV becomes worse due to the fact that the malicious jammer has more chances to attack the legal communication system at shorter distance between the jammer and UAV, exept for $(x_{\mathcal{S}_1}, y_{\mathcal{S}_1}) = (100, 0)$. Here, the IOP for $\mathcal{S}_1$ decreases significantly when $(x_{\mathcal{S}_1}, y_{\mathcal{S}_1}) = (0, 0)$ due to the fact that $\mathcal{S}_1$ has a better channel than $\mathcal{S}_2$ to be decoded first with less interference from the jammer.

Fig. 6 depicts the effects of both source nodes' positions on the IOPs with $m_1 = m_2 = m_{\mathcal{J}} = 3$, $\mu_1 = \mu_2' = 0.15$, $(x_u, y_u) = (40, 0)$, $y_{\mathcal{S}_2} = 0$, and $(x_{\mathcal{J}}, y_{\mathcal{J}}) = (100, 0)$. From the figure, we have the following observations:

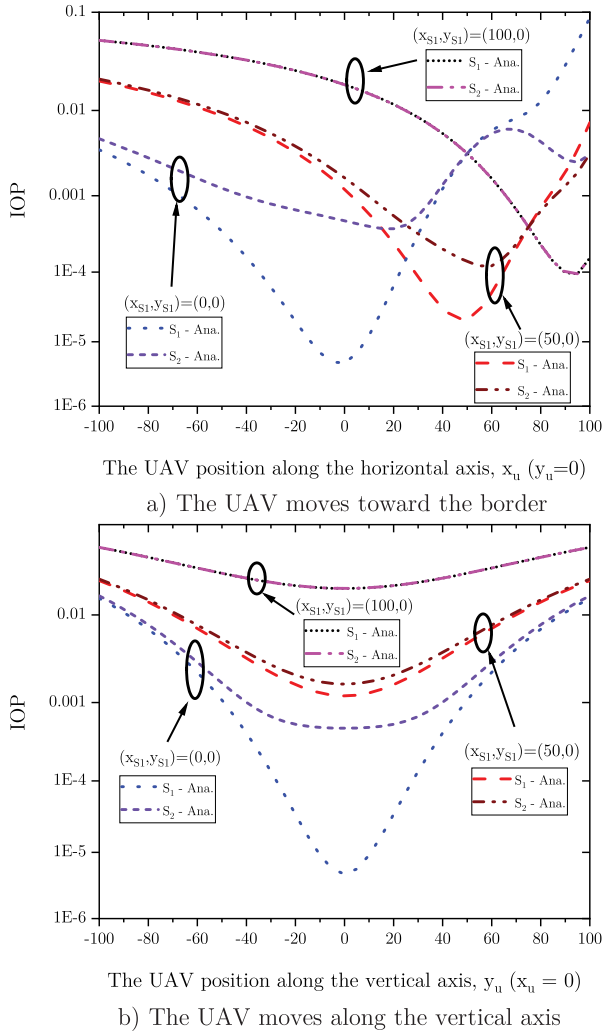


**FIGURE 5.** The effect of the UAV placement on the IOPs.

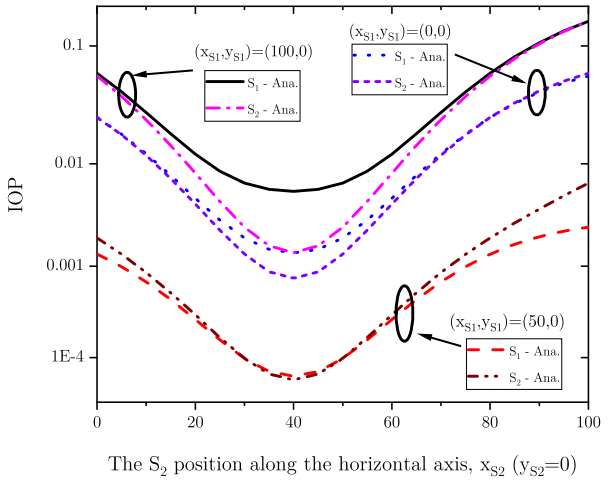


**FIGURE 6.** The effect of the two source node placements on the IOPs.

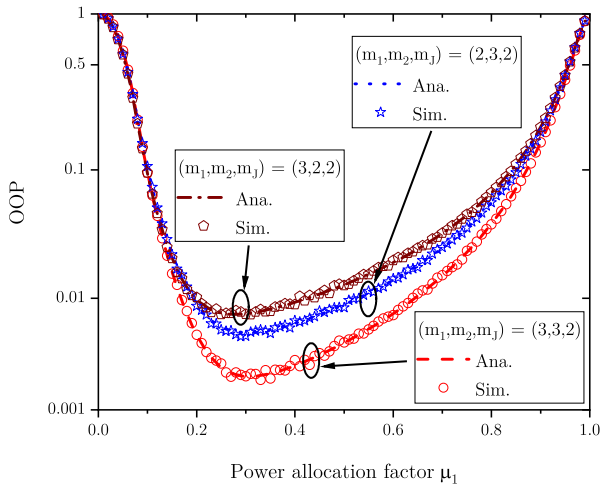


**FIGURE 7.** The validation of the calculations of the OOPs in different environments ($m_1, m_2, m_{\mathcal{J}}$).

- When $\mathcal{S}_2$ stays far away from the border as well as far from the UAV, the IOPs of both source nodes experience a significant increase due to the higher path-loss. Moreover, the communication reliability between the UAV and both source nodes is improved dramatically when the UAV keeps staying on top around $\mathcal{S}_2$ placement as explained earlier.
- When the second source node position is close to the border, the IOPs of both source nodes grow dramatically also due to the higher path-loss.
- We can see an interesting result in which the communication reliability between the UAV and both source nodes becomes significantly worse when both source nodes are situated close to the border. In contrast, the IOPs of both source nodes decrease dramatically when both source nodes stay far away from the border and of course they also depend on the UAV placement as discussed above. These results can suggest how to make a pair of source nodes to improve the communication reliability in the presence of jamming attack as provided in Section V-C.

### *B. OVERALL OUTAGE PROBABILITY*

In Fig. 7, the relationship between the OOP and the power allocation is highlighted in different environments represented by $(m_1, m_2, m_{\mathcal{J}})$ using the power allocation strategy of $\mu_1 = \mu_2'$, $(x_{\mathcal{S}_1}, y_{\mathcal{S}_1}) = (-100, 0)$, $(x_{\mathcal{S}_2}, y_{\mathcal{S}_2}) = (100, 0)$, $(x_{\mathcal{J}}, y_{\mathcal{J}}) = (150, 0)$, and $(x_u, y_u) = (-10, 0)$. Here, the match between simulation and analytical results very well validates the exactness of the calculation. We also can see that the effect of the power allocation factor on the OOP is significant. Therefore, finding the optimal power allocation plays an important role to improve the communication reliability in terms of minimizing the OOP. Furthermore, the communication reliability improves dramatically with a better environment $m_1 = m_2 = 3$.

By analyzing the effect of the jammer location on the OOP in different environments with $\mu_1 = \mu_2' = 0.1$, $(x_{\mathcal{S}_1}, y_{\mathcal{S}_1}) =$

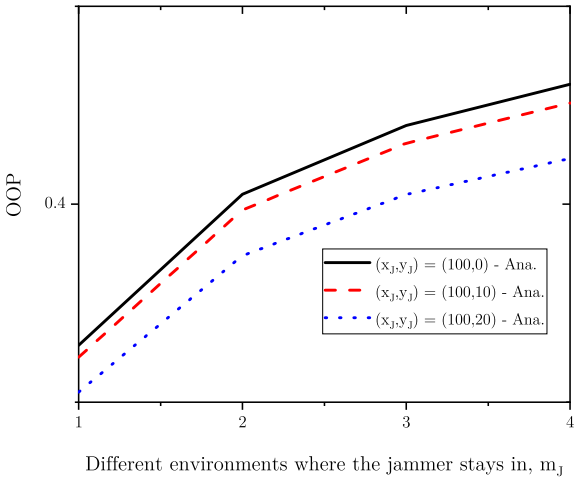


**FIGURE 8.** The effect of environment at the jammer location on the OOPs.

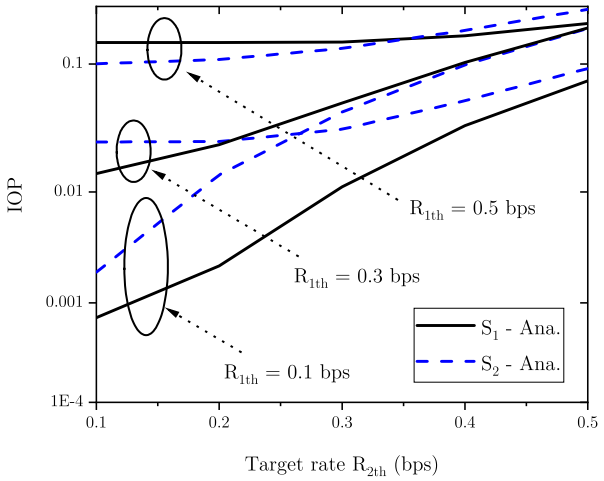


**FIGURE 9.** The effect of the target rates on the IOPs.

$(-100, 0)$, $(x_{\mathcal{S}_2}, y_{\mathcal{S}_2}) = (100, 0)$, and $(x_u, y_u) = (-10, 0)$, we can see that the OOP decreases dramatically when the malicious jammer moves along the horizontal axis far away from the border. This is because the distance between the UAV and jammer goes up significantly leading to a dramatic reduction of jamming attack effectiveness due to the higher path-loss. Moreover, when the jammer moves along the vertical axis, the jammer may make a chance to attack the legitimate UAV with the highest effectiveness by finding the smallest distance between itself and the UAV. On the other hand, we can limit the search space in terms of $(x_{\mathcal{J}min}, x_{\mathcal{J}max}, y_{\mathcal{J}min}, y_{\mathcal{J}max})$ for the proposed algorithms to find the optimal jammer placement in Section IV due to the fact that the search space of $(100 \leq x_{\mathcal{J}}, -\infty < y_{\mathcal{J}} < \infty)$ is not necessary for all contexts. Consequently, the number of iterations for the proposed algorithms can be decreased significantly.

Fig. 8 illustrates how the shape $m_{\mathcal{J}}$ affects the OOP with different jammer locations with $m_1 = m_2 = 3$, $\mu_1 = \mu_2' = 0.1$, $(x_{\mathcal{S}_1}, y_{\mathcal{S}_1}) = (-100, 0)$, $(x_{\mathcal{S}_2}, y_{\mathcal{S}_2}) = (100, 0)$, and $(x_u, y_u) = (0, 0)$. It can be seen from the figure that the OOP increases significantly for all jammer placements where the jammer experiences the better environments. This is a good point for the smart jammer to find the optimal jammer location attacking the legitimate system as well as to define the search space for the proposed algorithms in Section IV.

By investigating the effect of the UAV placement on the OOP in different environments with $\mu_1 = \mu_2' = 0.1$, $(x_{\mathcal{S}_1}, y_{\mathcal{S}_1}) = (-100, 0)$, $(x_{\mathcal{S}_2}, y_{\mathcal{S}_2}) = (100, 0)$, and $(x_{\mathcal{J}}, y_{\mathcal{J}}) = (150, 0)$, it can be seen that the distance between the UAV and the jammer along the horizontal axis affects significantly the communication reliability in terms of the OOP, e.g., at the border $x_u \approx 100$. In contrast, the OOP decreases significantly with an increase of this distance. However, if the UAV moves much further away from the border into the isolated area, the OOP goes up again due to the higher path-loss between the UAV and $\mathcal{S}_2$. When the UAV flies along the vertical axis, the OOP goes down significantly when the UAV placement is around the point belonging to the line connecting the two source nodes. As a result, the UAV location also keeps a crucial role to enhance the communication reliability. Moreover, we also can define a proper search space for the proposed algorithms in Section IV to find the optimal UAV placement in terms of minimizing the OOP. This contributes to a reduction of the number of iterations for the proposed algorithms. Consequently, given the effect of the jammer position on the OOP above, it is clear that both the UAV and the jammer can find strategies to optimize their own objectives.

We also investigate the effect of both source nodes placements on the OOP with $\mu_1 = \mu_2' = 0.1$, $(x_{\mathcal{J}}, y_{\mathcal{J}}) = (150, 50)$, and $(x_u, y_u) = (-100, 50)$. We can see that the OOP reduces significantly when $\mathcal{S}_2$ is located at the positions with $x_{\mathcal{S}_2} \approx x_u$ due to the effect of the path-loss. Therefore, making a pair of nodes plays an important role contributing to an improvement of the communication reliability. In particular, we should make a pair of two nodes locating far away from the border as much as possible. In the worst case, one node locating far away from the border is paired with another node locating next to the border.

Fig. 9 illustrates the effect of the target rates on the IOPs with $(m_1, m_2, m_{\mathcal{J}}) = (3, 3, 2)$, $\mu_1 = \mu_2' = 0.4$, $(x_{\mathcal{S}_1}, y_{\mathcal{S}_1}) = (-100, 0)$, $(x_{\mathcal{S}_2}, y_{\mathcal{S}_2}) = (100, 0)$, $(x_{\mathcal{J}}, y_{\mathcal{J}}) = (150, 0)$, and $(x_u, y_u) = (-10, 0)$. It can be seen from the figure that both IOPs grow significantly with an increase of the target rates. This suggests how to choose the target rate for each source node based on their timeliness and reliability requirements. For the OOP, we also can see the same phenomenon.

In Fig. 10, we use the same settings as we used for Fig. 3 with the case of $(m_1, m_2, m_{\mathcal{J}}) = (3, 3, 2)$ to make a comparison of the IOPs with and without a jammer. Here, when $P_{\mathcal{J}}$ is small enough, e.g., $P_{\mathcal{J}} = 1$ mW, but can be any

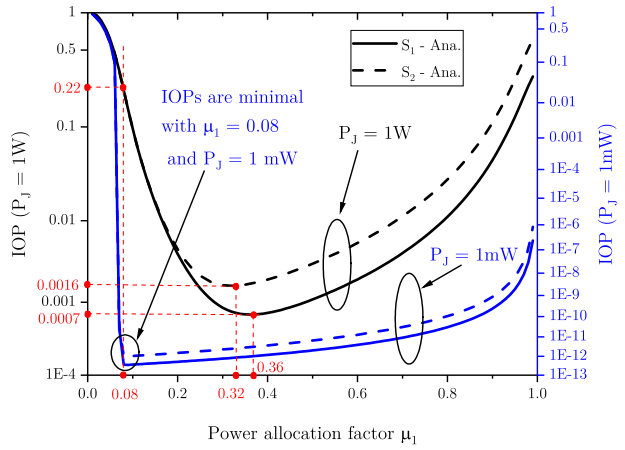


**FIGURE 10.** The comparison of the IOPs versus the power allocation between with and without a jammer.

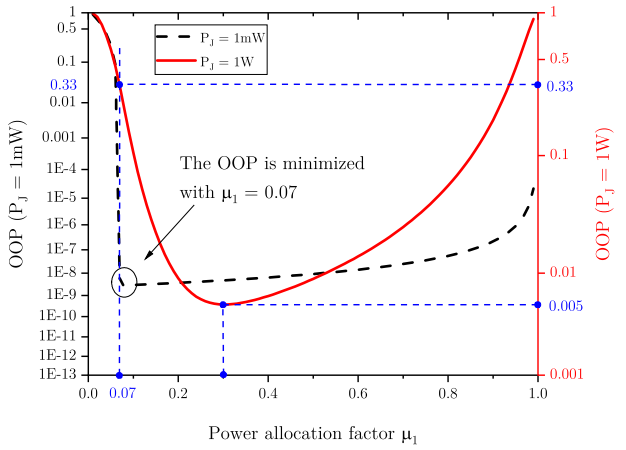


**FIGURE 12.** The comparison of the OOP versus the power allocation between with and without a jammer with $(m_1, m_2, m_{\mathcal{J}}) = (2, 3, 2)$.

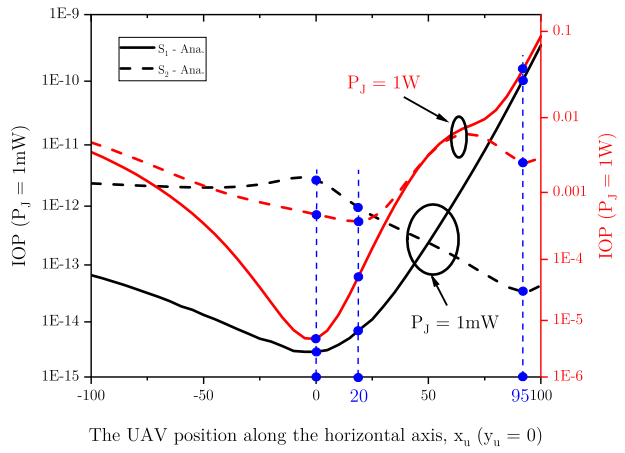


**FIGURE 11.** The comparison of the IOPs versus the UAV placement between with and without a jammer.

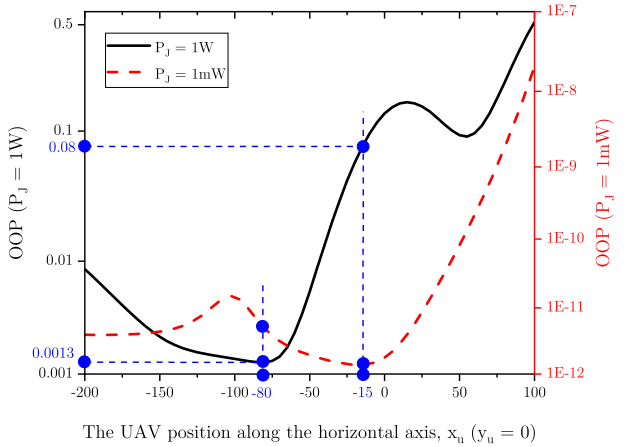


**FIGURE 13.** The comparison of the OOP versus the UAV placement between with and without a jammer with $(m_1, m_2, m_{\mathcal{J}}) = (3, 3, 2)$.

type of interferer. It can be seen from the figure that both IOPs are minimized with $\mu_1 \approx 0.08$ without any jammer present. If the power allocation does not adapt accordingly when a real jammer appears, the communication reliability is degraded dramatically, e.g., $p_i \approx 0.22$. In contrast, if the power allocation changes adaptively to the presence of a jammer with high jammer transmit power, it leads to a significant improvement of the communication reliability as shown in Fig. 10. Similarly, using the same setting in Fig. 5 with $(x_{\mathcal{S}_1}, y_{\mathcal{S}_1}) = (0, 0)$, we can see that a change of the UAV placement in the presence of the jamming attack is necessary to improve the communication reliability as shown in Fig. 11.

With the OOP, we also utilize the same setting investigating the effects of the power allocation and UAV placement on the OOP above to see how the OOP considering a jammer presence compared to the case without any jammer as shown in Figs. 12 and 13. From these results, a joint power allocation and UAV placement can help to improve the communication of the legitimate system in the presence jamming attack.

### 1) SCENARIO I: FIXED JAMMER

Adopting the proposed hybrid SA-Greedy as shown in Algorithm 1, the optimal power allocation for both power allocation strategies is provided in Fig. 14 with $m_1 = m_2 = m_{\mathcal{J}} = 3$, $P_{\mathcal{J}} = 0.5$W, $(x_{\mathcal{S}_1}, y_{\mathcal{S}_1}) = (-100, 0)$, $(x_{\mathcal{S}_2}, y_{\mathcal{S}_2}) = (100, 0)$, $(x_{\mathcal{J}}, y_{\mathcal{J}}) = (100, 0)$, and $(x_u, y_u) = (-50, 0)$. By experiment, we see that the obtained solution for both OOP and power allocation factors using the power allocation strategy $\mu_1 = \mu_2'$ takes less iterations ($N_1 = 100$), compared to the power allocation strategy $\mu_1 \neq \mu_2'$ ($N_1 = 3000$). It can be seen from the figure that the differences between the optimal OOPs using both power allocation strategies are very subtle in different environments. Therefore, the power allocation strategy $\mu_1 = \mu_2'$ with only one pair of power allocation should be used to reduce the computational load and time at the UAV and we use this power allocation strategy to find the optimal power allocation and UAV placement for both scenarios mentioned in Section IV.

The optimal power allocation and UAV placement versus $\mathcal{S}_2$'s location for the first scenario is provided in Table 4

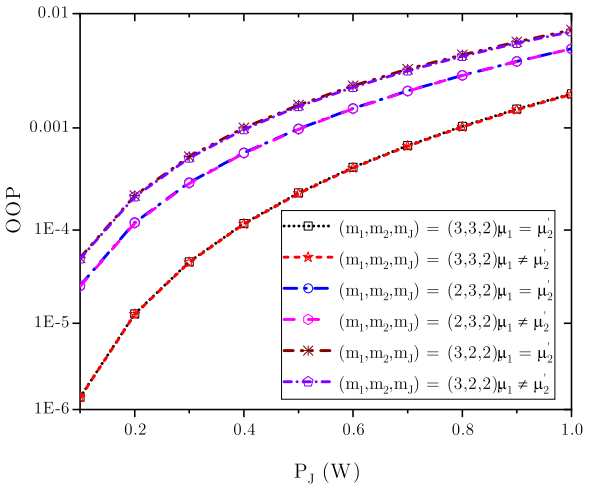


**FIGURE 14.** A comparison of the OOP among the two power allocation strategies in different environments.

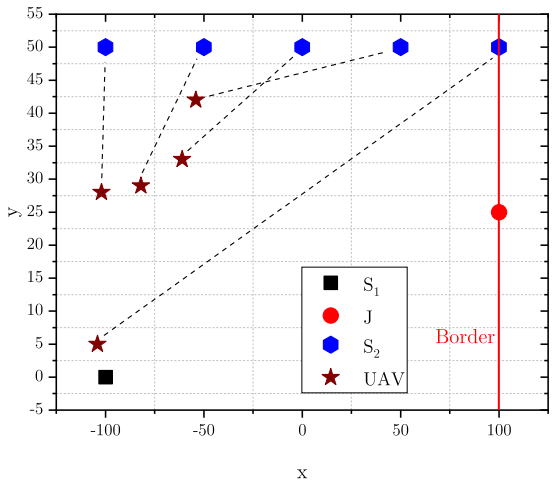


**FIGURE 15.** The optimal UAV placement versus $\mathcal{S}_2$'s location for the scenario I.

**TABLE 4.** The optimal power allocation and UAV placement versus $\mathcal{S}_2$'s location for the scenario I.

| $(x_{\mathcal{S}_2}, y_{\mathcal{S}_2})$ | (-100,50) | (-50,50) | (0,50) | (50,50) | (100,50) |
|---|---|---|---|---|---|
| $(x_u, y_u)$ | (-102,28) | (-82,29) | (-61,33) | (-54,42) | (-104,5) |
| $p$ | 2.56e-8 | 2.21e-7 | 5.77e-6 | 1.01e-4 | 5.58e-4 |
| $\mu_1$ | 0.143 | 0.846 | 0.194 | 0.785 | 0.064 |

**TABLE 5.** The optimal power allocation and UAV placement versus the jammer location for the scenario I.

| $(x_{\mathcal{J}}, y_{\mathcal{J}})$ | (100,25) | (125,25) | (150,25) | (175,25) | (200,25) |
|---|---|---|---|---|---|
| $(x_u, y_u)$ | (-104,5) | (-97,9) | (-44,42) | (-29,43) | (-21,36) |
| $p$ | 5.58e-4 | 2.93e-4 | 1.53e-4 | 6.98e-5 | 3.33e-5 |
| $\mu_1$ | 0.064 | 0.079 | 0.801 | 0.785 | 0.787 |

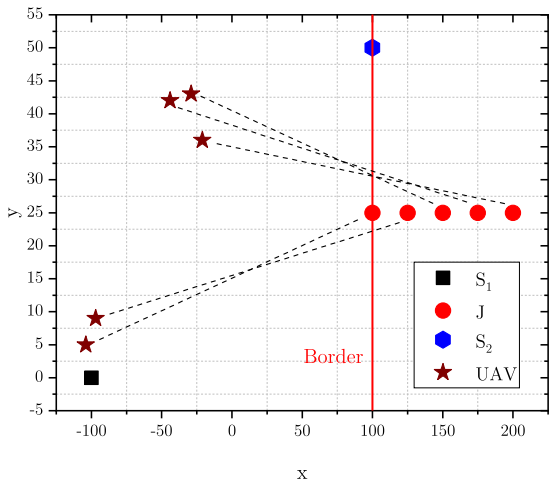


**FIGURE 16.** The optimal UAV placement versus the jammer location for the scenario I.

with $P_{\mathcal{J}} = 0.5$W, $m_1 = m_2 = m_{\mathcal{J}} = 3$, $(x_{\mathcal{S}_1}, y_{\mathcal{S}_1}) = (-100, 0)$, $(x_{\mathcal{J}}, y_{\mathcal{J}}) = (100, 25)$, $N_1 = 100$, and $N_2 = 100$. We can see that even with the optimal power allocation, the OOP increases significantly when $\mathcal{S}_2$ goes along the horizontal axis toward the border. Particularly, both source nodes locating far away from the border with $(x_{\mathcal{S}_2}, y_{\mathcal{S}_2}) = (-100, 50)$ can improve the communication reliability with $p = 2.56e-8$, while the OOP is much higher with $p = 5.58e-4$ when both source nodes locate at the border. This is useful to make a pair of source nodes as stated above. Moreover, the optimal UAV placement shifts slowly toward close to $\mathcal{S}_2$ when $\mathcal{S}_2$ moves toward the border as illustrated in Fig. 15. This can decrease the effect of the higher path-loss between the UAV and $\mathcal{S}_2$. However, when $\mathcal{S}_2$ is situated at the border, the optimal UAV location is close to $\mathcal{S}_1$. This position avoids disturbance from the distant malicious jammer and makes the communication link between the UAV and $\mathcal{S}_1$ better, as much more power is allocated for $\mathcal{S}_2$ experiencing the higher path-loss, $\mu_1 = 0.064$, Table 4.

Table 5 provides the optimal power allocation and UAV placement with different jammer locations for the first scenario, $P_{\mathcal{J}} = 0.5$W, $m_1 = m_2 = m_{\mathcal{J}} = 3$, $(x_{\mathcal{S}_1}, y_{\mathcal{S}_1}) = (-100, 0)$, $(x_{\mathcal{S}_2}, y_{\mathcal{S}_2}) = (100, 50)$, $N_1 = 100$, and $N_2 = 100$. We can see that when the malicious jammer moves away from the border, the optimal OOP decreases significantly. Moreover, the optimal UAV placement keeps being close to $\mathcal{S}_1$ to reduce the effect of the jamming attack when the jammer is still close to the border, Fig. 16. In contrast, the optimal UAV placement shifts to being close to $\mathcal{S}_2$ to decrease the effect of the higher path-loss between the UAV and $\mathcal{S}_2$ when the jammer stays far enough from the border.

Table 6 shows how the optimal power allocation and UAV placement change following the target rates for the first scenario, $P_{\mathcal{J}} = 0.5$W, $m_1 = m_2 = m_{\mathcal{J}} = 3$, $(x_{\mathcal{S}_1}, y_{\mathcal{S}_1}) = (-100, 0)$, $(x_{\mathcal{S}_2}, y_{\mathcal{S}_2}) = (100, 50)$, $(x_{\mathcal{J}}, y_{\mathcal{J}}) = (100, 25)$, $N_1 = 100$, and $N_2 = 100$. It can be seen from the table that an increase of the target rate results in a growth of the optimal OOP. Moreover, when the target rate $R_{2th}$ goes up, the optimal UAV placement adapts by shifting away from $\mathcal{S}_1$. Fig. 17 shows an example from Table 6 for $R_{1th} = 0.1$, where the clear movement up along the vertical axis away from $\mathcal{S}_1$ is visible. In contrast, the optimal UAV location

**TABLE 6.** The optimal power allocation and UAV placement versus the target rates of both source nodes for the scenario I.

| $R_{1th}$ | $R_{2th}$=0.1 | $R_{2th}$=0.2 | $R_{2th}$=0.3 | $R_{2th}$=0.4 | $R_{2th}$=0.5 |
|---|---|---|---|---|---|
| 0.1 | (-104,4), 5.58e-4, 0.937 | (-104,6), 3.8e-3, 0.04 | (-105,8), 11.5e-3, 0.968 | (-105,10), 24.9e-3, 0.972 | (-106,12), 44.4e-3, 0.026 |
| 0.2 | (-103,2), 6.46e-4, 0.905 | (-103,3), 4.2e-3, 0.065 | (-104,5), 12.4e-3, 0.05 | (-104,5), 26.4e-3, 0.042 | (-104,6), 46.7e-3, 0.963 |
| 0.3 | (-103,1), 7.37e-4, 0.128 | (-103,2), 4.5e-3, 0.083 | (-104,3), 13.2e-3, 0.935 | (-104,4), 27.7e-3, 0.945 | (-104,4), 48.6e-3, 0.952 |
| 0.4 | (-103,1), 8.32e-4, 0.156 | (-103,2), 4.9e-3, 0.897 | (-103,2), 13.9e-3, 0.92 | (-103,3), 29e-3, 0.932 | (-103,4), 50.5e-3, 0.06 |
| 0.5 | (-102,1), 9.32e-4, 0.818 | (-103,1), 5.3e-3, 0.88 | (-103,2), 14.7e-3, 0.096 | (-103,2), 30.3e-3, 0.92 | (-103,2), 52.3e-3, 0.072 |

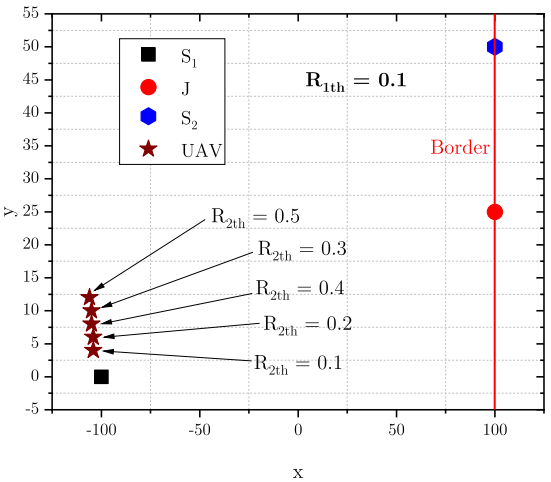


**FIGURE 17.** The effect of $R_{2th}$ on the optimal UAV placement for the scenario I with $R_{1th} = 0.1$.

moves closer to $\mathcal{S}_1$ with an increase of the target rate $R_{1th}$ as can be seen from the Table 6, e.g., with $R_{2th} = 0.5$.

Table 7 describes the smart jammer locations versus $\mathcal{S}_2$'s placements for the first scenario when equilibrium condition is obtained, $P_{\mathcal{J}} = 0.5$W, $m_1 = m_2 = m_{\mathcal{J}} = 3$, $(x_{\mathcal{S}_1}, y_{\mathcal{S}_1}) = (-100, 0)$, $N_1 = 100$, $N_2 = 100$, and $N_3 = 100$. We can see that the OOP increases slightly when the distance between the two source nodes goes up. Moreover, the smart jammer placement moves towards $\mathcal{S}_2$'s location at the border, Fig. 18. This is because the UAV should stay at the middle position compared to both source nodes to reduce the effect of the higher path-loss between the UAV and source nodes links and then the smart jammer also reacts adaptively. It is highlighted that the smart jammer locations are always at the border to decrease the effect of path-loss as much as possible for attacking.

### 2) SCENARIO II: MOBILE JAMMER

For the second scenario, Table 8 illustrates how the jammer placement changes with different UAV locations, $P_{\mathcal{J}} = 0.5$W, $m_1 = m_2 = 3$, $m_{\mathcal{J}} = 2$, $(x_{\mathcal{S}_1}, y_{\mathcal{S}_1}) = (-100, 0)$, $(x_{\mathcal{S}_2}, y_{\mathcal{S}_2}) = (100, 50)$, $N_1 = 100$, and $N_4 = 100$. The results

**TABLE 7.** The jammer placement versus $\mathcal{S}_2$'s location applying competition game for the scenario I.

| $(x_{\mathcal{S}_2}, y_{\mathcal{S}_2})$ | (100,0) | (100,25) | (100,50) | (100,75) | (100,100) |
|---|---|---|---|---|---|
| $(x_{\mathcal{J}}, y_{\mathcal{J}})$ | (100,0) | (100,4) | (100,7) | (100,29) | (100,47) |
| $p$ | 5.01e-4 | 5.18e-4 | 5.68e-4 | 6.48e-4 | 7.57e-4 |
| $\mu_1$ | 0.067 | 0.934 | 0.917 | 0.914 | 0.208 |

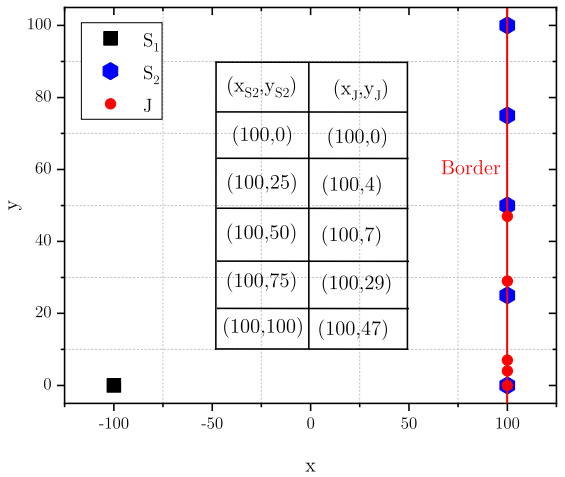


**FIGURE 18.** The jammer placement versus $\mathcal{S}_2$'s location applying non-cooperative game for the scenario I.

**TABLE 8.** The jammer placement versus the UAV location for the scenario II.

| $(x_u, y_u)$ | (-75,10) | (-50,20) | (-25,30) | (0,40) | (25,50) |
|---|---|---|---|---|---|
| $(x_{\mathcal{J}}, y_{\mathcal{J}})$ | (100,9) | (100,21) | (100,30) | (100,40) | (100,50) |
| $p$ | 8.79e-4 | 1.2e-3 | 1.7e-3 | 4.7e-3 | 31e-3 |
| $\mu_1$ | 0.889 | 0.81 | 0.723 | 0.331 | 0.307 |

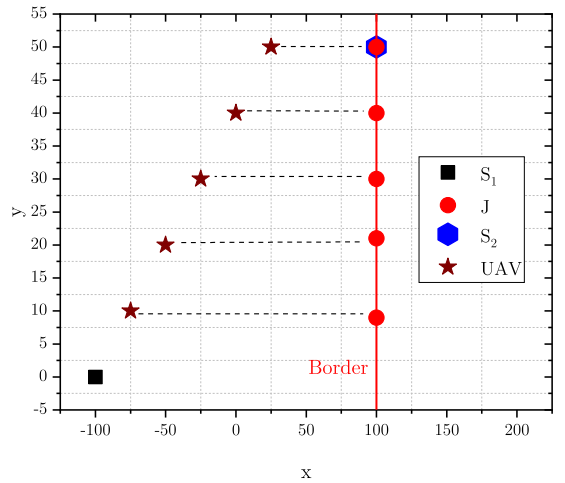


**FIGURE 19.** The jammer location with different UAV placements for the scenario II.

show that the OOP goes up significantly when the distance between the UAV and the border decreases. Importantly, the tendency of the smart jammer's optimal location is to reduce the distance between the UAV and the jammer as much as possible, decreasing the effect of path-loss, Fig. 19. This can help to limit the search space as well as reduce number of iterations to find the optimal jammer placement as discussed above.

**TABLE 9.** The power allocation and UAV placement versus $\mathcal{S}_2$'s location for the scenario II.

| $(x_{\mathcal{S}_2}, y_{\mathcal{S}_2})$ | (-100,0) | (-50,0) | (0,0) | (50,0) | (100,0) |
|---|---|---|---|---|---|
| $(x_u, y_u)$ | (-105,25) | (-81,22) | (-60,19) | (-53,15) | (-105,39) |
| $p$ | 2.26e-8 | 2.21e-7 | 5.81e-6 | 1.04e-4 | 5.69e-4 |
| $\mu_1$ | 0.869 | 0.154 | 0.807 | 0.211 | 0.077 |

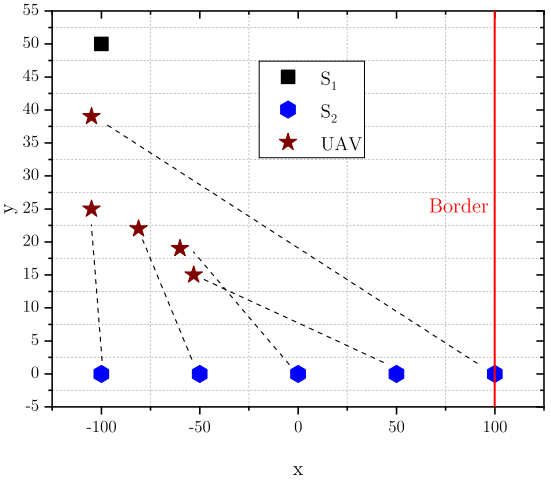


**FIGURE 20.** The effect of $\mathcal{S}_2$'s location on the UAV placement for the scenario II.

The power allocation and UAV placement for the second scenario with different $\mathcal{S}_2$'s locations is provided in Table 9, $P_{\mathcal{J}} = 0.5$W, $m_1 = m_2 = m_{\mathcal{J}} = 3$, $(x_{\mathcal{S}_1}, y_{\mathcal{S}_1}) = (-100, 50)$, $N_1 = 100$, $N_4 = 100$, and $N_5 = 100$. It can be seen that the communication reliability in terms of the OOP increases dramatically when $\mathcal{S}_2$ keeps staying far away from the border. To ensure high communication reliability, the UAV also locates itself far away from the border as shown in Fig. 20. We can see that the optimal UAV placement moves toward to $\mathcal{S}_2$ when $\mathcal{S}_2$ is closer to the border. However, when the distance between $\mathcal{S}_2$ and the border is quite small, e.g., $(x_{\mathcal{S}_2}, y_{\mathcal{S}_2}) = (100, 0)$, the UAV will stay close to $\mathcal{S}_1$ and allocate more power for $\mathcal{S}_2$ to improve the communication reliability.

Finally, the power allocation and UAV placement versus the change of both target rates are presented in Table 10 with $P_{\mathcal{J}} = 0.5$W, $m_1 = m_2 = m_{\mathcal{J}} = 3$, $(x_{\mathcal{S}_1}, y_{\mathcal{S}_1}) = (-100, 50)$, $(x_{\mathcal{S}_2}, y_{\mathcal{S}_2}) = (100, 0)$, $N_1 = 100$, $N_4 = 100$, and $N_5 = 100$. In general, the optimal OOP increases with an increase of the target rate. In most cases, the UAV always keeps a position far away from the border to reduce the effect of the jamming attack. When the target rate of one source node increases, the optimal UAV placement is shifted close to this source node to make the communication link between the UAV and this node better, Fig. 21. Then, more power is assigned for $\mathcal{S}_2$ to overcome the higher path-loss with an increase of $R_{2th}$, while the power level for $\mathcal{S}_1$ also goes up slightly with an increase of the target rate $R_{1th}$.

### C. DISCUSSIONS

Based on the obtained results, the following guidelines can be provided:

**TABLE 10.** The power allocation and UAV placement versus the target rates of both source nodes for the scenario II.

| $R_{1th}$ | $R_{2th}$=0.1 | $R_{2th}$=0.2 | $R_{2th}$=0.3 | $R_{2th}$=0.4 | $R_{2th}$=0.5 |
|---|---|---|---|---|---|
| 0.1 | (-105,39), 5.69e-4, 0.924 | (-104,40), 3.9e-3, 0.956 | (-105,37), 11.7e-3, 0.037 | (-105,35), 25.1e-3, 0.033 | (-107,33), 44.7e-3, 0.969 |
| 0.2 | (-103,45), 6.65e-4, 0.899 | (-103,44), 4.3e-3, 0.067 | (-104,42), 12.6e-3, 0.053 | (-105,40), 26.8e-3, 0.047 | (-105,39), 47.3e-3, 0.042 |
| 0.3 | (-103,47), 7.61e-4, 0.871 | (-103,45), 4.7e-3, 0.914 | (-103,44), 13.5e-3, 0.068 | (-104,42), 28.3e-3, 0.94 | (-104,42), 49.5e-3, 0.053 |
| 0.4 | (-103,47), 8.59e-4, 0.158 | (-103,46), 5.1e-3, 0.898 | (-103,45), 14.3e-3, 0.083 | (-104,44), 29.6e-3, 0.072 | (-103,43), 51.5e-3, 0.936 |
| 0.5 | (-103,48), 9.64e-4, 0.818 | (-103,47), 5.4e-3, 0.878 | (-103,46), 15.1e-3, 0.906 | (-103,45), 31.0e-3, 0.083 | (-103,44), 53.5e-3, 0.074 |

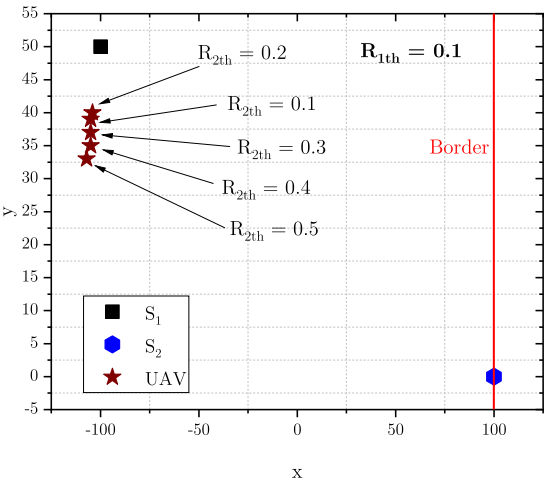


**FIGURE 21.** The effect of $R_{2th}$ on the UAV placement for the scenario II with $R_{1th} = 0.1$.

- The power allocation strategy $\mu_1 = \mu_2'$ with only one pair of power allocations can offer a communication reliability close to the power allocation strategy $\mu_1 \neq \mu_2'$ with two pairs of power allocations. Therefore, the power allocation strategy $\mu_1 = \mu_2'$ is used to reduce the computational load at the UAV.
- When creating pairs of source nodes, we should not make a pair of both source nodes close to the border, i.e., at least one source far away from the border.
- Based on the effects of locations of both the UAV and a malicious jammer on the OOP, we can limit the search space for the proposed algorithms in Section IV. This contributes to a reduction of the number of iterations required to find the optimal power allocation and UAV placement faster.
- The UAV has the tendency to stay around the middle between the source nodes to keep balance in the path-loss on the links between the UAV and the sources. However, when one source node is located close to the border, the UAV leans to the other one which is far away from the border following the second guideline.

## VI. CONCLUSION

In this work we look at a scenario including one UAV communicating with two source nodes in uplink pairwise NOMA in the presence of a jamming attack. First, calculations of exact closed-form expressions of both OOP and IOP considering imperfect CSI over a Nakagami-$m$ fading channel are provided. Next, we formulate a non-cooperative game for the UAV and a smart jammer based on their conflict of interest in terms of communication reliability. Accordingly, we propose a set of hybrid SA-Greedy algorithms to solve the joint power allocation and UAV placement problem for two scenarios: fixed and mobile jammer. Once the Nash equilibrium points are obtained, the UAV should fly directly to that position and keep staying there to reduce its power consumption. Thereafter, we investigate the effect of a wide range of parameters such as power allocation, source node placements, UAV placement, target rates, and jammer location on the outage performance. We also make a comparison to show how the communication reliability gains when adapting the power allocation and the UAV placement to the presence of the jammer compared to keeping the power allocation and UAV placement obtained when considering the jammer as an interferer. The results indicate how to select a power allocation strategy, make pairs of source nodes, choose parameters for the proposed algorithms to reduce the number of iterations in order to improve the communication reliability as well as to decrease the complexity of the communication protocol and computational load. As future work, we would like to take imperfect SIC, hardware impairment, mobile source nodes and Doppler effect into account when looking at both offline and online algorithms for dealing with jamming attacks, including several cooperative smart jammers.

## APPENDIX

*Theorem 2:* Given three random variables $X \sim G(m_X, \frac{\rho_X}{m_X})$, $Y \sim G(m_Y, \frac{\rho_Y}{m_Y})$, and $Z \sim G(m_Z, \frac{\rho_Z}{m_Z})$ where $m_X$, $m_Y$, and $m_Z$ are positive integers, the closed-form expressions of the probability $p = \Pr\{(Z \geq \alpha_1 Y + \alpha_2 X + \alpha_3) \cap (Y \geq \alpha_4 X + \alpha_5) \cap (X \geq \alpha_6)\}$, where $(\alpha_1, \alpha_2, \alpha_3, \alpha_4, \alpha_5, \alpha_6)$ are constant, can be derived as follows:

(a) $\alpha_1 \neq 0, \alpha_2 = 0, \alpha_3 = 0, \alpha_4 \neq 0, \alpha_5 \neq 0$:

$$p_a = \frac{\left(m_Y\rho_Y^{-1}\right)^{m_Y}\left(m_X\rho_X^{-1}\right)^{m_X} e^{-A_0\alpha_5}}{\Gamma(m_X)\Gamma(m_Y)} \times \sum_{j=0}^{m_Z-1} \frac{\left(m_Z\rho_Z^{-1}\alpha_1\right)^j \Gamma(m_Y+j)}{j!A_0^{m_Y+j}} \sum_{l=0}^{m_Y+j-1} \frac{A_0^l}{l!} \times \sum_{q=0}^{l} \binom{l}{q} \alpha_4^q \alpha_5^{l-q} \frac{\Gamma(m_X+q, B_0\alpha_6)}{B_0^{m_X+q}}, \tag{56}$$

(b) $\alpha_1 \neq 0, \alpha_2 \neq 0, \alpha_3 \neq 0, \alpha_4 = 0, \alpha_5 = 0, \alpha_6 = 0$:

$$p_b = \frac{\left(m_Y\rho_Y^{-1}\right)^{m_Y}\left(m_X\rho_X^{-1}\right)^{m_X} e^{-m_Z\rho_Z^{-1}\alpha_3}}{\Gamma(m_X)\Gamma(m_Y)} \times \sum_{i=0}^{m_Z-1} \frac{\left(m_Z\rho_Z^{-1}\right)^i}{i!} \sum_{j=0}^{i} \binom{i}{j} \alpha_1^j \sum_{k=0}^{i-j} \alpha_3^{i-j-k}\alpha_2^k \times \binom{i-j}{k} \frac{\Gamma(m_Y+j)}{A_0^{m_Y+j}} \frac{\Gamma(m_X+k)}{C_0^{m_X+k}}, \tag{57}$$

(c) $\alpha_1 \neq 0, \alpha_2 \neq 0, \alpha_3 \neq 0, \alpha_4 \neq 0, \alpha_5 \neq 0, \alpha_6 = 0$:

$$p_c = \frac{\left(m_Y\rho_Y^{-1}\right)^{m_Y}\left(m_X\rho_X^{-1}\right)^{m_X} e^{-m_Z\rho_Z^{-1}\alpha_3 - A_0\alpha_5}}{\Gamma(m_X)\Gamma(m_Y)} \times \sum_{i=0}^{m_Z-1} \frac{\left(m_Z\rho_Z^{-1}\right)^i}{i!} \sum_{j=0}^{i} \binom{i}{j} \frac{\alpha_1^j \Gamma(m_Y+j)}{A_0^{m_Y+j}} \times \sum_{k=0}^{i-j} \alpha_3^{i-j-k}\alpha_2^k \binom{i-j}{k} \sum_{l=0}^{m_Y+j-1} \frac{A_0^l}{l!} \times \sum_{q=0}^{l} \binom{l}{q} \alpha_5^{l-q}\alpha_4^q \frac{\Gamma(m_X+k+q)}{D_0^{m_X+k+q}}, \tag{58}$$

where $A_0 = m_Y\rho_Y^{-1} + m_Z\rho_Z^{-1}\alpha_1$, $B_0 = m_X\rho_X^{-1} + A_0\alpha_4$, $C_0 = m_X\rho_X^{-1} + m_Z\rho_Z^{-1}\alpha_2$, and $D_0 = m_X\rho_X^{-1} + m_Z\rho_Z^{-1}\alpha_2 + A_0\alpha_4$.

*Proof:* The cumulative distribution function and probability density function of the random variable $X \sim G(m_X, \frac{\rho_X}{m_X})$, $Y \sim G(m_Y, \frac{\rho_Y}{m_Y})$, and $Z \sim G(m_Z, \frac{\rho_Z}{m_Z})$ are given as follows, respectively:

$$F_V(v) = 1 - \frac{\Gamma\left(m_V, m_V\rho_V^{-1}v\right)}{\Gamma(m_V)}, v > 0, \tag{59}$$

$$f_V(v) = \frac{\left(m_V\gamma_V^{-1}\right)^{m_V} t^{m_V-1}e^{-m_V\gamma_V^{-1}t}}{\Gamma(m_V)}, v > 0, \tag{60}$$

where $V \in \{X, Y, Z\}$ and $v \in \{x, y, z\}$.

$$\begin{aligned} p &= \int_{\alpha_6}^{\infty} f_X(x)dx \int_{\alpha_4 x+\alpha_5}^{\infty} f_Y(y)dy \int_{\alpha_1 y+\alpha_2 x+\alpha_3}^{\infty} f_Z(z)dz \\ &= \frac{\left(m_Y\rho_Y^{-1}\right)^{m_Y}}{\Gamma(m_Y)} \int_{\alpha_6}^{\infty} f_X(x)dx \int_{\alpha_4 x+\alpha_5}^{\infty} y^{m_Y-1}e^{-m_Y\rho_Y^{-1}y} \times \frac{\Gamma\left(m_Z, m_Z\rho_Z^{-1}(\alpha_1 y + \alpha_2 x + \alpha_3)\right)}{\Gamma(m_Z)}dy, \end{aligned} \tag{61}$$

(a) $\alpha_1 \neq 0, \alpha_2 = 0, \alpha_3 = 0, \alpha_4 \neq 0, \alpha_5 \neq 0$: From (61), applying [62, eq. (8.352.4)], [62, eq. (3.381.3)], [62, eq. (8.352.4)], [62, eq. (1.111)], and [62, eq. (3.381.3)] in order, $p_a$ is derived as in (56).

(b) $\alpha_1 \neq 0, \alpha_2 \neq 0, \alpha_3 \neq 0, \alpha_4 = 0, \alpha_5 = 0, \alpha_6 = 0$: From (61), applying [62, eq. (8.352.4)], [62, eq. (1.111)], [62, eq. (1.111)], [62, eq. (3.381.3)], and [62, eq. (3.381.3)] in order, $p_b$ is derived as in (57).

(c) $\alpha_1 \neq 0, \alpha_2 \neq 0, \alpha_3 \neq 0, \alpha_4 \neq 0, \alpha_5 \neq 0, \alpha_6 = 0$: From (61), applying [62, eq. (8.352.4)], [62, eq. (1.111)], [62, eq. (3.381.3)], [62, eq. (1.111)], [62, eq. (8.352.4)], [62, eq. (1.111)], and [62, eq. (3.381.3)] in order, $p_c$ is derived as in (58). ■

### A. PROOF OF LEMMA 1

In this sub-section, the closed-form expressions of the probabilities $I_{11}$, $I_{12}$, $I_{21}$, and $I_{22}$ are derived using the Venn diagram method [16].

$I_{11}$ can be calculated as follows:

$$I_{11} = \begin{cases} I_{11a} & a_5 < a_7, x_1 \le 0 \\ I_{11b} & a_5 \ge a_7, x_1 > 0 \\ 0 & a_5 \ge a_7, x_1 \le 0 \\ I_{11c} & a_5 < a_7, x_1 > 0, \end{cases} \tag{62}$$

in which $I_{11a}$, $I_{11b}$, and $I_{11c}$ are given as

$$\begin{aligned} I_{11a} &= \Pr\{(h_1 > a_1h_2 + a_2h_{\mathcal{J}} + a_3) \\ &\qquad \cap (h_2 > a_4h_{\mathcal{J}} + a_5) \cap (h_2 < a_6h_{\mathcal{J}} + a_7)\} \\ &= \Pr\{(h_1 > a_1h_2 + a_2h_{\mathcal{J}} + a_3) \cap (h_2 > a_4h_{\mathcal{J}} + a_5)\} \\ &\quad - \Pr\{(h_1 > a_1h_2 + a_2h_{\mathcal{J}} + a_3) \\ &\qquad \cap (h_2 > a_6h_{\mathcal{J}} + a_7)\} \\ &= I_{10} - \Pr\left\{\begin{matrix}(h_1 > a_1h_2 + a_2h_{\mathcal{J}} + a_3) \\ \cap (h_2 > a_6h_{\mathcal{J}} + a_7)\end{matrix}\right\}, \end{aligned} \tag{63}$$

$$\begin{aligned} I_{11b} &= \Pr\{(h_{\mathcal{J}} > x_1) \cap (h_1 > a_1h_2 + a_2h_{\mathcal{J}} + a_3) \\ &\qquad \cap (h_2 > a_4h_{\mathcal{J}} + a_5) \cap (h_2 < a_6h_{\mathcal{J}} + a_7)\} \\ &= \Pr\{(h_{\mathcal{J}} > x_1) \cap (h_2 > a_4h_{\mathcal{J}} + a_5) \\ &\qquad \cap (h_1 > a_1h_2 + a_2h_{\mathcal{J}} + a_3)\} \\ &\quad - \Pr\{(h_{\mathcal{J}} > x_1) \cap (h_2 > a_6h_{\mathcal{J}} + a_7) \\ &\qquad \cap (h_1 > a_1h_2 + a_2h_{\mathcal{J}} + a_3)\}, \end{aligned} \tag{64}$$

$$I_{11c} = I_{11a} - I_{11b}, \tag{65}$$

Applying Theorem 2, $I_{11}$ is attained as in (21).

$I_{12}$ can be calculated as follows:

$$I_{12} = \begin{cases} I_{12a} & a_5 \ge a_7, x_1 \le 0 \\ I_{12b} & a_5 < a_7, x_1 \le 0 \\ I_{12c} & a_5 \ge a_7, x_1 > 0 \\ I_{12d} & a_5 < a_7, x_1 > 0, \end{cases} \tag{66}$$

in which $I_{12a}$, $I_{12b}$, $I_{12c}$, and $I_{12d}$ are defined as

$$I_{12a} = \Pr\{(h_2 > a_4h_{\mathcal{J}} + a_5) \cap (h_1 \ge h_2)\}, \tag{67}$$

$$I_{12b} = \Pr\{(h_2 > a_6h_{\mathcal{J}} + a_7) \cap (h_1 \ge h_2)\}, \tag{68}$$

$$I_{12c} = I_{12a} - Q_1, \tag{69}$$

where

$$\begin{aligned} Q_1 &= \Pr\{(h_{\mathcal{J}} \ge x_1) \cap (h_2 > a_4h_{\mathcal{J}} + a_5) \cap (h_1 \ge h_2)\} \\ &\quad - \Pr\{(h_{\mathcal{J}} \ge x_1) \cap (h_2 > a_6h_{\mathcal{J}} + a_7) \\ &\qquad \cap (h_1 \ge h_2)\}, \end{aligned} \tag{70}$$

$$I_{12d} = I_{12b} + Q_1. \tag{71}$$

Applying Theorem 2, $I_{12}$ is derived as in (24).

$I_{21}$ can be expressed as follows:

$$I_{21} = \begin{cases} I_{21a} & b_5 < b_7, x_2 \le 0 \\ I_{21b} & b_5 \ge b_7, x_2 > 0 \\ 0 & b_5 \ge b_7, x_2 \le 0 \\ I_{21c} & b_5 < b_7, x_2 > 0, \end{cases} \tag{72}$$

in which $I_{21a}$, $I_{21b}$, and $I_{21c}$ are given as

$$I_{21a} = I_{20} - \Pr\left\{\begin{matrix}(h_1 > b_6h_{\mathcal{J}} + b_7) \cap \\ (h_2 > b_1h_1 + b_2h_{\mathcal{J}} + b_3)\end{matrix}\right\}, \tag{73}$$

$$\begin{aligned} I_{21b} &= \Pr\{(h_1 > b_4h_{\mathcal{J}} + b_5) \cap (h_{\mathcal{J}} > x_2) \\ &\qquad \cap (h_2 > b_1h_1 + b_2h_{\mathcal{J}} + b_3)\} \\ &\quad - \Pr\{(h_{\mathcal{J}} > x_2) \cap (h_1 > b_6h_{\mathcal{J}} + b_7) \\ &\qquad \cap (h_2 > b_1h_1 + b_2h_{\mathcal{J}} + b_3)\}, \end{aligned} \tag{74}$$

$$I_{21c} = I_{21a} - I_{21b}. \tag{75}$$

Applying Theorem 2, $I_{21}$ is attained as in (29).

Similar to the way calculating $I_{12}$, $I_{22}$ can be calculated as follows:

$$I_{22} = \begin{cases} I_{22a} & b_5 \ge b_7, x_2 \le 0 \\ I_{22b} & b_5 < b_7, x_2 \le 0 \\ I_{22c} & b_5 \ge b_7, x_2 > 0 \\ I_{22d} & b_5 < b_7, x_2 > 0, \end{cases} \tag{76}$$

in which $I_{22a}$, $I_{22b}$, $I_{22c}$, and $I_{22d}$ are defined as

$$I_{22a} = \Pr\{(h_2 > h_1) \cap (h_1 > b_4h_{\mathcal{J}} + b_5)\}, \tag{77}$$

$$I_{22b} = \Pr\{(h_2 > h_1) \cap (h_1 > b_6h_{\mathcal{J}} + b_7)\}, \tag{78}$$

$$I_{22c} = I_{22a} - Q_2, \tag{79}$$

where

$$\begin{aligned} Q_2 &= \Pr\{(h_2 > h_1) \cap (h_1 > b_4h_{\mathcal{J}} + b_5) \cap (h_{\mathcal{J}} > x_1)\} \\ &\quad - \Pr\{(h_2 > h_1) \cap (h_1 > b_6h_{\mathcal{J}} + b_7) \cap (h_{\mathcal{J}} \ge x_1)\}, \end{aligned} \tag{80}$$

$$I_{22d} = I_{22b} + Q_2. \tag{81}$$

Applying Theorem 2, $I_{22}$ is derived as in (32).

### B. PROOF OF LEMMA 2

$I_{8b}$ can be rewritten as follows:

$$\begin{aligned} I_{8b} &= I_{8a} + I_{11a} - I_{10} \\ &\quad + \Pr\{(h_1 \ge h_2) \cap (h_2 > a_6h_{\mathcal{J}} + a_7)\}. \end{aligned} \tag{82}$$

Applying Theorem 2, this lemma is proved.

### C. PROOF OF LEMMA 3

We can rewrite $I_{9b}$ as follows:

$$\begin{aligned} I_{9b} &= I_{9a} + I_{21a} - I_{20} \\ &\quad + \Pr\{(h_2 > h_1) \cap (h_1 > b_6h_{\mathcal{J}} + b_7)\}. \end{aligned} \tag{83}$$

Applying Theorem 2, this lemma is proved.

## REFERENCES


[1] H. Wang *et al.*, "Architectural design alternatives based on cloud/edge/fog computing for connected vehicles," *IEEE Commun. Surveys Tuts.*, vol. 22, no. 4, pp. 2349–2377, 4th Quart., 2020.

[2] M. Mozaffari, W. Saad, M. Bennis, Y.-H. Nam, and M. Debbah, "A tutorial on UAVs for wireless networks: Applications, challenges, and open problems," *IEEE Commun. Surveys Tuts.*, vol. 21, no. 3, pp. 2334–2360, 3rd Quart., 2019.

[3] R. Shakeri *et al.*, "Design challenges of multi-UAV systems in cyber-physical applications: A comprehensive survey and future directions," *IEEE Commun. Surveys Tuts.*, vol. 21, no. 4, pp. 3340–3385, 4th Quart., 2019.

[4] V. Chamola, V. Hassija, V. Gupta, and M. Guizani, "A comprehensive review of the COVID-19 pandemic and the role of IoT, drones, AI, blockchain, and 5G in managing its impact," *IEEE Access*, vol. 8, pp. 90225–90265, 2020.

[5] T. Do-Duy, L. D. Nguyen, T. Q. Duong, S. Khosravirad, and H. Claussen, "Joint optimisation of real-time deployment and resource allocation for UAV-aided disaster emergency communications," *IEEE J. Sel. Areas Commun.*, early access, Jun. 14, 2021, doi: 10.1109/JSAC.2021.3088662.

[6] V. Semkin, E. M. Vitucci, F. Fuschini, M. Barbiroli, V. Degli-Esposti, and C. Oestges, "Characterizing the UAV-to-machine UWB radio channel in smart factories," *IEEE Access*, vol. 9, pp. 76542–76550, 2021.

[7] A. Caruso, S. Chessa, S. Escolar, J. Barba, and J. C. López, "Collection of data with drones in precision agriculture: Analytical model and LoRa case study," *IEEE Internet Things J.*, early access, Apr. 26, 2021, doi: 10.1109/JIOT.2021.3075561.

[8] Z. Ma, M. Xiao, Y. Xiao, Z. Pang, H. V. Poor, and B. Vucetic, "High-reliability and low-latency wireless communication for Internet of Things: Challenges, fundamentals, and enabling technologies," *IEEE Internet Things J.*, vol. 6, no. 5, pp. 7946–7970, Oct. 2019.

[9] T. Lennvall, M. Gidlund, and J. Åkerberg, "Challenges when bringing IoT into industrial automation," in *IEEE AFRICON*, Cape Town, South Africa, 2017, pp. 905–910.

[10] M. Kaneko, I. Randrianantenaina, H. Dahrouj, H. Elsawy, and M. S. Alouini, "On the opportunities and challenges of NOMA-based fog radio access networks: An overview," *IEEE Access*, vol. 8, pp. 205467–205476, 2020.

[11] X. Liu and X. Zhang, "NOMA-based resource allocation for cluster-based cognitive industrial Internet of Things," *IEEE Trans. Ind. Informat.*, vol. 16, no. 8, pp. 5379–5388, Aug. 2020.

[12] Y. Yuan, Y. Zhao, B. Zong, and S. Parolari, "Potential key technologies for 6G mobile communications," *Sci. China Inf. Sci.*, vol. 63, pp. 1–19, May 2020.

[13] Y. Liu, Z. Qin, and Z. Ding, *Non-Orthogonal Multiple Access for Massive Connectivity*. Cham, Switzerland: Springer, 2020.

[14] J. Montalban, E. Iradier, P. Angueira, O. Seijo, and I. Val, "NOMA-based 802.11n for industrial automation," *IEEE Access*, vol. 8, pp. 168546–168557, 2020.

[15] L. Dai, B. Wang, Y. Yuan, S. Han, I. Chih-Lin, and Z. Wang, "Non-orthogonal multiple access for 5G: Solutions, challenges, opportunities, and future research trends," *IEEE Commun. Mag.*, vol. 53, no. 9, pp. 74–81, Sep. 2015.

[16] V.-L. Dao, L.-N. Hoang, S. Girs, and E. Uhlemann, "Outage performance of pairwise NOMA allowing a dynamic decoding order and optimal pairs of power levels," *IEEE Open J. Commun. Soc.*, vol. 1, pp. 1886–1906, 2020.

[17] M. Raza, N. Aslam, H. Le-Minh, S. Hussain, Y. Cao, and N. M. Khan, "A critical analysis of research potential, challenges, and future directives in industrial wireless sensor networks," *IEEE Commun. Surveys Tuts.*, vol. 20, no. 1, pp. 39–95, 1st Quart., 2018.

[18] A. Mpitziopoulos, D. Gavalas, C. Konstantopoulos, and G. Pantziou, "A survey on jamming attacks and countermeasures in WSNs," *IEEE Commun. Surveys Tuts.*, vol. 11, no. 4, pp. 42–56, 4th Quart., 2009.

[19] V. N. Vo, C. So-In, H. Tran, D.-D. Tran, and T. P. Huu, "Performance analysis of an energy-harvesting IoT system using a UAV friendly jammer and NOMA under cooperative attack," *IEEE Access*, vol. 8, pp. 221986–222000, 2020.

[20] National Institute of Standards and Technology. *Reactive Jamming Attack*. Accessed: Jun. 15, 2021. [Online]. Available: https://nvd.nist.gov/vuln/search/results?form_type=Basic&results_type=overview&query=wireless+jamming+attack&search_type=all

[21] X. Sun, F. R. Yu, and P. Zhang, "A survey on cyber-security of connected and autonomous vehicles (CAVs)," *IEEE Trans. Intell. Transp. Syst.*, early access, Jun. 7, 2021, doi: 10.1109/TITS.2021.3085297.

[22] T. P. Raptis, A. Passarella, and M. Conti, "A survey on industrial Internet with ISA100 wireless," *IEEE Access*, vol. 8, pp. 157177–157196, 2020.

[23] T. Gebremichael *et al.*, "Security and privacy in the industrial Internet of Things: Current standards and future challenges," *IEEE Access*, vol. 8, pp. 152351–152366, 2020.

[24] B. Leander, A. Čaušević, and H. Hansson, "Applicability of the IEC 62443 standard in industry 4.0 / IIoT," in *Proc. Int. Conf. Availability Rel. Security*, 2019, pp. 1–8. [Online]. Available: https://doi.org/10.1145/3339252.3341481

[25] F. Pan, Z. Pang, M. Luvisotto, M. Xiao, and H. Wen, "Physical-layer security for industrial wireless control systems: Basics and future directions," *IEEE Ind. Electron. Mag.*, vol. 12, no. 4, pp. 18–27, Dec. 2018.

[26] "Cisco annual Internet report (2018–2023)," Cisco, San Jose, CA, USA, White Paper, Mar. 2020. [Online]. Available: https://www.cisco.com/c/en/us/solutions/collateral/executive-perspectives/annual-internet-report/white-paper-c11-741490.html

[27] K. Yang, "Interference management in LTE wireless networks [industry perspectives]," *IEEE Wireless Commun.*, vol. 19, no. 3, pp. 8–9, Jun. 2012.

[28] A. Willig, K. Matheus, and A. Wolisz, "Wireless technology in industrial networks," *Proc. IEEE*, vol. 93, no. 6, pp. 1130–1151, Jun. 2005.

[29] S. Yan, X. Cao, Z. Liu, and X. Liu, "Interference management in 6G space and terrestrial integrated networks: Challenges and approaches," *Intell. Converged Netw.*, vol. 1, no. 3, pp. 271–280, Dec. 2020.

[30] V. N. Vo, H. Tran, V.-L. Dao, C. So-In, D.-D. Tran, and E. Uhlemann, "On communication performance in energy harvesting WSNs under a cooperative jamming attack," *IEEE Syst. J.*, vol. 14, no. 4, pp. 4955–4966, Dec. 2020.

[31] H. Wang, Y. Fu, R. Song, Z. Shi, and X. Sun, "Power minimization precoding in uplink multi-antenna NOMA systems with jamming," *IEEE Trans. Green Commun. Netw.*, vol. 3, no. 3, pp. 591–602, Sep. 2019.

[32] A. Alipour-Fanid, M. Dabaghchian, and K. Zeng, "Impact of jamming attacks on vehicular cooperative adaptive cruise control systems," *IEEE Trans. Veh. Technol.*, vol. 69, no. 11, pp. 12679–12693, Nov. 2020.

[33] S. Hosseinalipour, A. Rahmati, and H. Dai, "Optimal jammer placement in UAV-assisted relay networks," in *Proc. IEEE Int. Conf. Commun.*, Dublin, Ireland, 2020, pp. 1–6.

[34] J. Feng, W. E. Dixon, T. F. Wong, and J. M. Shea, "Optimal jammer placement in the real plane to partition a wireless network," in *Proc. IEEE Wireless Commun. Netw. Conf.*, Marrakesh, Morocco, 2019, pp. 1–7.

[35] S. Gezici, S. Bayram, M. N. Kurt, and M. R. Gholami, "Optimal jammer placement in wireless localization systems," *IEEE Trans. Signal Process.*, vol. 64, no. 17, pp. 4534–4549, Sep. 2016.

[36] S. Vadlamani, B. Eksioglu, H. Medal, and A. Nandi, "Jamming attacks on wireless networks: A taxonomic survey," *Int. J. Prod. Econ.*, vol. 172, pp. 76–94, Feb. 2016. [Online]. Available: https://www.sciencedirect.com/science/article/pii/S092552731500451X

[37] Q. Wu, W. Mei, and R. Zhang, "Safeguarding wireless network with UAVs: A physical layer security perspective," *IEEE Wireless Commun.*, vol. 26, no. 5, pp. 12–18, Oct. 2019.

[38] B. Duan, D. Yin, Y. Cong, H. Zhou, X. Xiang, and L. Shen, "Anti-jamming path planning for unmanned aerial vehicles with imperfect jammer information," in *Proc. IEEE Int. Conf. Robot. Biomimetics*, Kuala Lumpur, Malaysia, 2018, pp. 729–735.

[39] J. Åkerberg, M. Gidlund, and M. Björkman, "Future research challenges in wireless sensor and actuator networks targeting industrial automation," in *Proc. 9th IEEE Int. Conf. Ind. Informat.*, Lisbon, Portugal, 2011, pp. 410–415.

[40] Iskandar and S. Shimamoto, "The channel characterization and performance evaluation of mobile communication employing stratospheric platform," in *Proc. IEEE/ACES Int. Conf. Wireless Commun. Appl. Comput. Electromagn.*, Honolulu, HI, USA, 2005, pp. 828–831.

[41] Y. Liu, Z. Ding, M. Elkashlan, and H. V. Poor, "Cooperative non-orthogonal multiple access with simultaneous wireless information and power transfer," *IEEE J. Sel. Areas Commun.*, vol. 34, no. 4, pp. 938–953, Apr. 2016.

[42] Z. Ding, Z. Yang, P. Fan, and H. V. Poor, "On the performance of non-orthogonal multiple access in 5G systems with randomly deployed users," *IEEE Signal Process. Lett.*, vol. 21, no. 12, pp. 1501–1505, Dec. 2014.

[43] X. Li, Q. Wang, Y. Liu, T. A. Tsiftsis, Z. Ding, and A. Nallanathan, "UAV-aided multi-way NOMA networks with residual hardware impairments," *IEEE Wireless Commun. Lett.*, vol. 9, no. 9, pp. 1538–1542, Sep. 2020.

[44] A. Goldsmith, *Wireless Communications*. Boston, MA, USA: Cambridge Univ. Press, 2005.
[45] S. S. Ikki and S. Aissa, "Two-way amplify-and-forward relaying with Gaussian imperfect channel estimations," *IEEE Commun. Lett.*, vol. 16, no. 7, pp. 956–959, Jul. 2012.
[46] Z. Ding, R. Schober, and H. V. Poor, "A general MIMO framework for NOMA downlink and uplink transmission based on signal alignment," *IEEE Trans. Wireless Commun.*, vol. 15, no. 6, pp. 4438–4454, Jun. 2016.
[47] Y. Gao, B. Xia, Y. Liu, Y. Yao, K. Xiao, and G. Lu, "Analysis of the dynamic ordered decoding for uplink NOMA systems with imperfect CSI," *IEEE Trans. Veh. Technol.*, vol. 67, no. 7, pp. 6647–6651, Jul. 2018.
[48] P. Xu, Z. Yang, Z. Ding, and Z. Zhang, "Optimal relay selection schemes for cooperative NOMA," *IEEE Trans. Veh. Technol.*, vol. 67, no. 8, pp. 7851–7855, Aug. 2018.
[49] N. Zhang, J. Wang, G. Kang, and Y. Liu, "Uplink nonorthogonal multiple access in 5G systems," *IEEE Commun. Lett.*, vol. 20, no. 3, pp. 458–461, Mar. 2016.
[50] E. K. Burke and G. Kendall, Eds., *Search Methodologies: Introductory Tutorials in Optimization and Decision Support Techniques*, 2nd ed. New York, NY, USA: Springer, 2014.
[51] W. Wang *et al.*, "Energy-constrained UAV-assisted secure communications with position optimization and cooperative jamming," *IEEE Trans. Commun.*, vol. 68, no. 7, pp. 4476–4489, Jul. 2020.
[52] H. V. Abeywickrama, B. A. Jayawickrama, Y. He, and E. Dutkiewicz, "Comprehensive energy consumption model for unmanned aerial vehicles, based on empirical studies of battery performance," *IEEE Access*, vol. 6, pp. 58383–58394, 2018.
[53] W. Aldosari, M. Zohdy, and R. Olawoyin, "Jammer localization through smart estimation of jammer's transmission power," in *Proc. IEEE Nat. Aerosp. Electron. Conf.*, Dayton, OH, USA, USA, 2019, pp. 430–436.
[54] Y. Gong, W. Xu, L. Guo, Z. Zhang, and P. Zhang, "Trajectory-curvature-aware moving jammer positioning for UAV networks," in *Proc. 11th Int. Conf. Wireless Commun. Signal Process.*, Xi'an, China, 2019, pp. 1–6.
[55] E.-G. Talbi, *Metaheuristics: From Design to Implementation*. Hoboken, NJ, USA: Wiley, 2009.
[56] Y. G. Saab and V. B. Rao, "Combinatorial optimization by stochastic evolution," *IEEE Trans. Comput.-Aided Design Integr. Circuits Syst.*, vol. 10, no. 4, pp. 525–535, Apr. 1991.
[57] C. D. Aliprantis and K. C. Border, *Infinite Dimensional Analysis: A Hitchhiker's Guide*, 2nd ed. Heidelberg, Germany: Springer, 1999.
[58] Z. Han, D. Niyato, W. Saad, and T. Başar, *Game Theory for Next Generation Wireless and Communication Networks: Modeling, Analysis, and Design*. Cambridge, U.K.: Cambridge Univ. Press, 2019.
[59] M. J. Osborne and A. Rubinstein, *A Course in Game Theory* (MIT Press Books), vol. 1. Cambridge, MA, USA: MIT Press, Sep. 1994. [Online]. Available: https://ideas.repec.org/b/mtp/titles/0262650401.html
[60] H. Tabassum, M. S. Ali, E. Hossain, M. J. Hossain, and D. I. Kim, "Uplink vs. downlink NOMA in cellular networks: Challenges and research directions," in *Proc. IEEE Veh. Technol. Conf.*, Sydney, NSW, Australia, 2017, pp. 1–7.
[61] X. Li, J. Li, Y. Liu, Z. Ding, and A. Nallanathan, "Residual transceiver hardware impairments on cooperative NOMA networks," *IEEE Trans. Wireless Commun.*, vol. 19, no. 1, pp. 680–695, Jan. 2020.
[62] I. S. Gradshteyn and I. M. Ryzhik, *Table of Integrals, Series, and Products*, 7th ed. Amsterdam, The Netherlands: Elsevier, 2007.

**VAN-LAN DAO** (Graduate Student Member, IEEE) received the B.S. degree in electrical and electronic engineering and the M.S. degree in automation and control engineering from the Le Quy Don Technical University, Ha Noi, Vietnam, in 2011 and 2016, respectively. He is currently pursuing the Ph.D. degree with the Data Communications Group, School of Innovation, Design and Engineering, Malardalen University, Västerås, Sweden. His research interests include embedded system design for Internet of Things, wireless sensor networks and wireless body area networks, hardware security, digital VLSI/ASIC design and FPGA-based system hardware design, non-orthogonal multiple access, timely and reliable communication for wireless networks, physical layer security, and game theory.

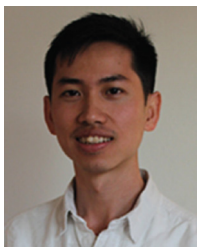

**LE-NAM HOANG** (Member, IEEE) received the B.Eng. degree in electronics and telecommunications from the Hanoi University of Science and Technology, Vietnam, in 2007, the M.Sc. degree in electrical engineering from the Blekinge Institute of Technology, Sweden, in 2010, and the Ph.D. degree in computer science and engineering from Halmstad University, Västerås, Sweden, in 2017. He is currently a Researcher with the School of Innovation, Design and Engineering, Malardalen University. His research interests include nonorthogonal multiple access and relaying strategies, under the constraints of timeliness, reliability and security, for wireless communications in critical applications.

**SVETLANA GIRS** (Member, IEEE) received the B.Sc. and M.Sc. degrees in telecommunications from Saint-Petersburg State Polytechnic University, Russia, from 2009 and 2011, respectively, and the Ph.D. degree in computer science and engineering from Malardalen University, Västerås, Sweden. She is a Lecturer with the School of Innovation, Design and Engineering, Malardalen University, where she is currently leading the Networked and Embedded Systems Division. She has been a Visiting Researcher with University of Canterbury, Christchurch, New Zealand, for three months in 2014. Her research interests include real-time communication, cooperative relay networks and reliable wireless communication for industrial systems. She is also a Co-chair of the Subcommittee on Industrial Communication Systems within the IEEE IES Technical Committee on Factory Automation.

**ELISABETH UHLEMANN** (Senior Member, IEEE) received the Ph.D. degree in communications theory from the Chalmers University of Technology, Gothenburg, Sweden, in 2004. She has held visiting positions with the University of South Australia in 2005, the Technical University of Berlin in 2007, and the University of Canterbury, New Zealand, in 2011. She has also worked as a Consultant with Volvo Technology from 2005 to 2009, dealing with connected vehicles, with Ikanos Communications, Fremont, CA, USA, in 2005, and with VDSL Protocols and Free2move, Sweden, from 2009 to 2010, with wireless audio. She is currently a Full Professor of Data Communications with Malardalen University, Sweden. She has been involved in several European projects studying communication requirements for traffic-safety applications in vehicular networks. She also contributed to the European ITS communications architecture and he has served as a Technical Expert in standardization within ETSI TC ITS. She currently serves as a Senior Editor for IEEE VEHICULAR TECHNOLOGY MAGAZINE on *Connected and Automated Vehicles*. She has served as a member of different Ph.D. examination committees over 20 times in five different countries.